Development of bioconjugates for targeted tumor therapy of cancer types leading to high mortality

1. Introduction

Targeted cancer therapy is a promising tool to overcome the drawbacks of classical chemotherapy like the lack of selectivity, toxicity to healthy tissue and the development of multidrug resistance forced by high dose treatments. In general, ligands with high binding affinities to tumor-specific receptors or receptors which are overexpressed on the surface of cancer cells can be used as carriers for anticancer drugs enabling the selective delivery of an effective cytotoxic agent or radionuclides to tumor cells. Peptide ligands provide valuable properties such as excellent tissue permeability, low immunogenicity and structural simplicity [1.]. In comparison to protein-based biopharmaceuticals like monoclonal antibodies, an additional benefit is that peptides can be produced cost-efficiently in large scale by chemical synthesis [2,3]. Especially, the good progress in peptide technology, solid phase synthesis and chemical ligation techniques facilitate the synthesis and modification of peptides [4,5]. Therefore, the search of new tumor homing peptides is a hot topic in targeted cancer therapy [6]. Next to the well-known receptors (*e.g.* peptide hormone receptors) that are overexpressed on tumor cells and applied commonly as targets [7], one of the approach often used to explore new peptides is a technique belonging to *in vitro* evolution methods: phage display is a useful tool to identify tumor specific peptides that can be used efficiently for anticancer drug targeting [8].The main problem of the application of peptide therapeutics is their relatively short plasma half-life and the corresponding *in vivo* stability. The proteolytic digestion of the peptides can be prevented or reduced by incorporating unnatural amino acids (*e.g.* D-amino acids) or peptide cyclization [9-11]. Replacing one or more amino acids with their D-version may not only enhance the proteolytic stability but also lead to an improved or reduced activity and/or receptor affinity of the compounds.

In our OTKA project (K119552), we focused on hormone peptide-based targeting moiety *e.g.* gonadotropin-releasing hormone (GnRH), neurotensin (NT) and bombesin (BB) as well as integrin-, CD13-, HER-2, Hsp-70-, and FRIZZ-receptor specific homing peptides selected by phage display. Our results are summarized below.

2. GnRH-based drug targeting for targeted tumor therapy

The aim of our first research was to achieve an improved inhibitory effect on the growth of cancer cells by incorporating various unnatural amino acids into the GnRH-III sequence. Based on previously reported antiproliferative activity studies of drug-free GnRH-III (Glp-His-Trp-Ser-His-Asp-Trp-Lys-Pro-Gly-NH$_2$, where Glp is pyroglutamic acid) derivatives [12], we synthesized and characterized a series of 14 novel GnRH-III-[^{8}Lys(Dau=Aoa)] (where Dau=Aoa is oxime-linked daunomycin through aminooxyacetyl moiety) conjugates [13]. Next to the influence of amino acid substitutions in position 3 and 7 by D-amino acids, the effect of changing the *C*-terminal region and the presence of a negative

charge in position six was studied. For a better comparison and to ensure that no cross interactions are caused, all selected changes were performed for two different groups of compounds, one group with the natural serine in position four and a second group where the serine was exchanged by butyrylated lysine. All synthesized conjugates were analyzed for their growth inhibitory effect on GnRH-R expressing MCF-7 human breast cancer and HT-29 human colon cancer cells. The best candidate was chosen for a detailed biochemical evaluation including stability in human plasma, lysosomal degradation in the presence of rat liver lysosomal homogenate, cellular uptake by flow cytometry and confocal laser scanning microscopy (CLSM) as well as receptor binding affinity.

The results indicated that the replacement of ^{3}Trp by ^{3}D-Tic (D-1,2,3,4-tetrahydroisoquinoline-3-carboxylic acid) in connection with the deletion of ^{2}His led to an increased cytostatic effect of conjugate (Glp-D-Tic-Lys(tBu)-His-Asp-Trp-Lys(Dau=Aoa)-Pro-Gly-NH$_2$ (**10**)) on the analyzed cell lines. The IC$_{50}$ value of bioconjugate **10** was more than 15-times lower on ER+ breast cancer MCF-7 cells and 5-times lower on colon cancer cells HT-29 compared to our previous lead compound **K2** (Glp-His-Trp-Lys(tBu)-His-Asp-Trp-Lys(Dau=Aoa)-Pro-Gly-NH$_2$) as control [14]. The IC$_{50}$ values were 0.14 ± 0.01 and 2.36 ± 0.07 (MCF-7) and 3.31 ± 0.90 and 15.93 ± 0.99 (HT-29), respectively. The increased antitumor activity could be explained by the higher cellular uptake of the new conjugate (**Figure 1**).
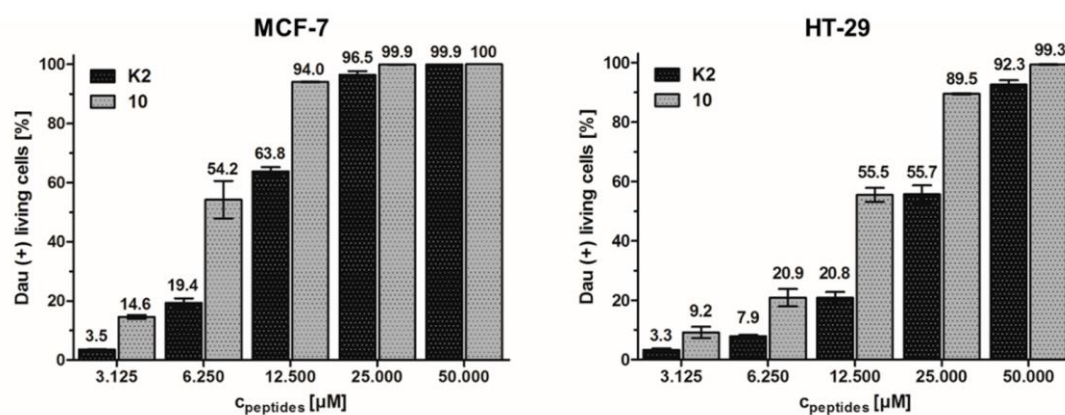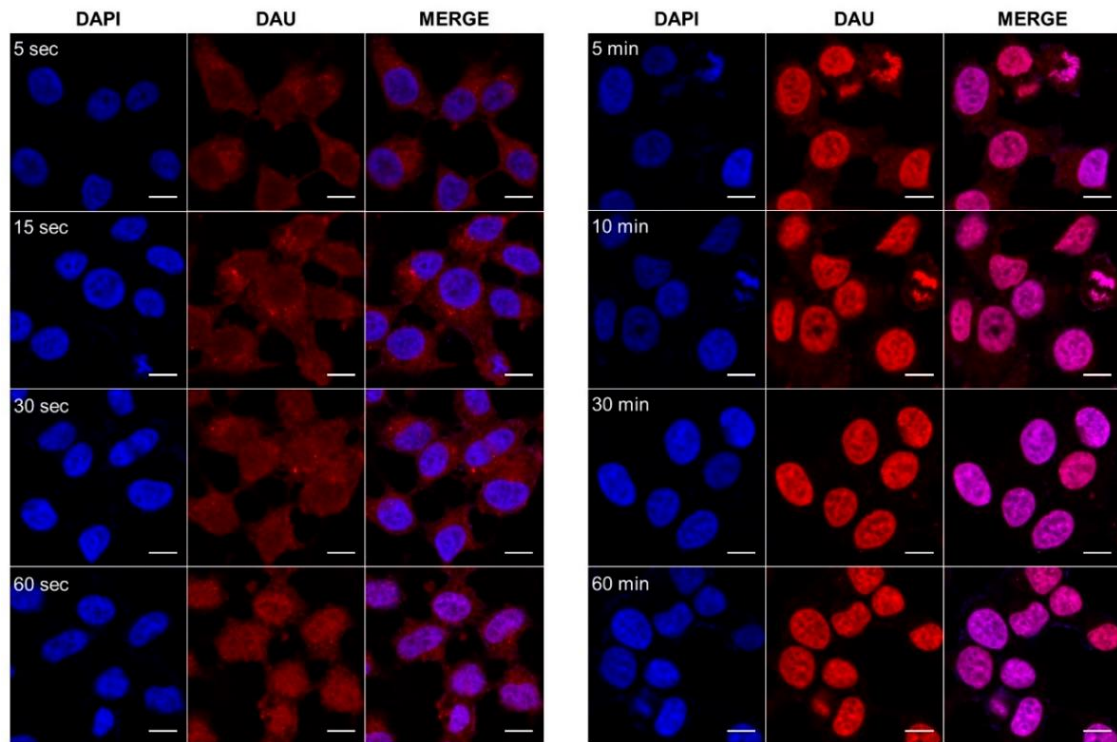

Figure 1. Cellular uptake of the GnRH-III conjugates **K2** and **10** on MCF-7 (left) and HT-29 (right) cancer cells after 6 h treatment determined by flow cytometry. The cellular uptake of 10 was significantly higher than the uptake of conjugate **K2** for both cells (paired Wilcoxon test, p = 0.004 and p = 0.005, respectively).

The time dependence and the mechanism of cellular uptake and the localization of the drug was also indicated by confocal laser scanning microscope (**Figure 2.** and **Figure 3.**). The results indicated that the new conjugate (**10**) enter faster into the cells and the Dau containing metabolite localized in the nucleus within 5 min instead of 30 min (**K2**).
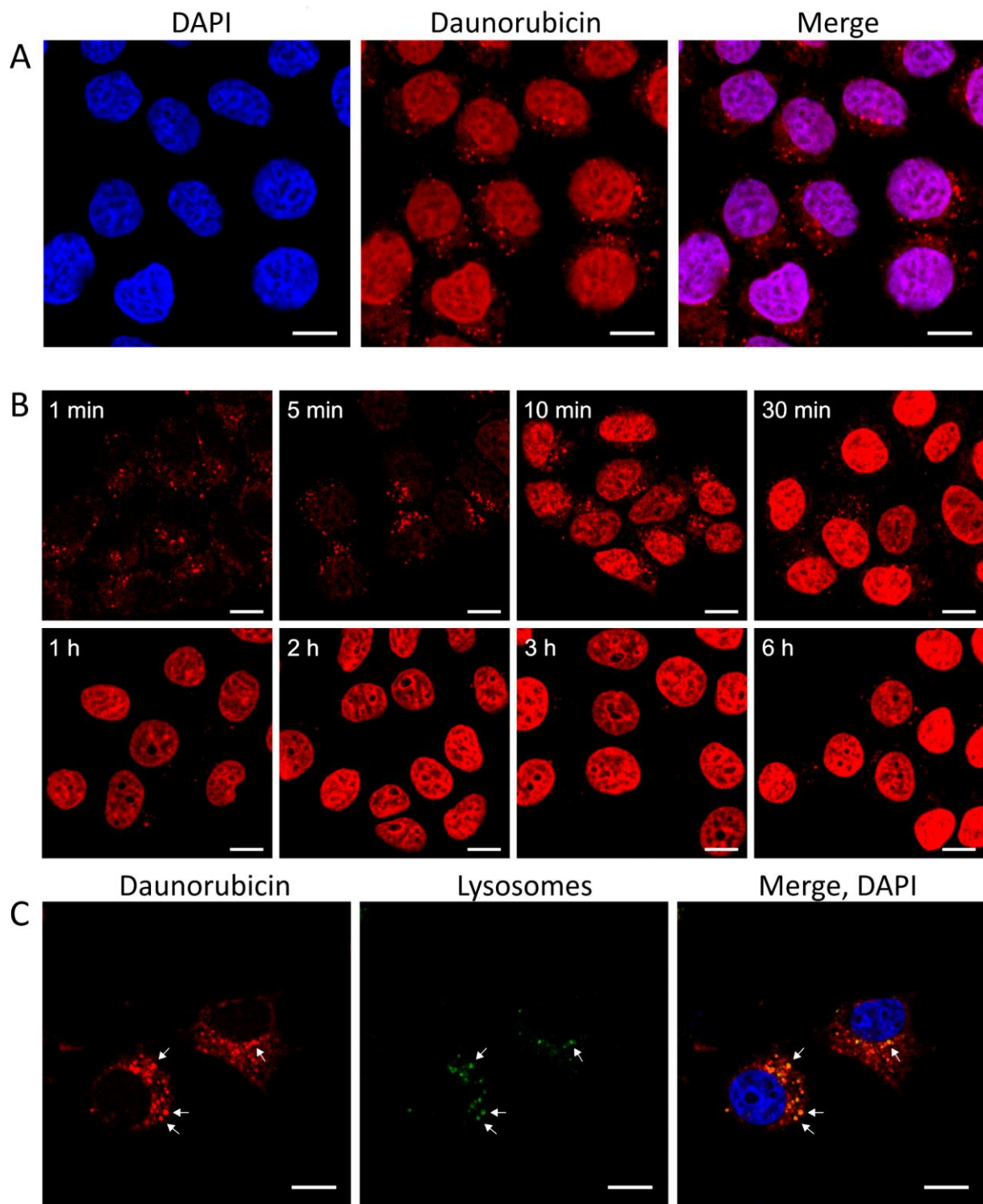
Figure 2. Cellular uptake of bioconjugate **K2** (40 μM) visualized by confocal laser scanning microscopy (CLSM) A) after 6 h incubation, daunorubicin (Dau) accumulates in the nucleus. B) Time dependent localization of bioconjugate **K2** after 1 min, 5 min, 10 min, 30 min, 1 h, 2 h, 3 h and 6 h incubation. C) Co-localization of **K2** (40 μM) with lysosomes (CytoPainter Lysosomal Staining Kit) after 5 min incubation. In the early stages of the cellular uptake the Dau signal is co-localized with the lysosomal staining (scale bars represent 10 μm).

Figure 3. Time-dependent cellular uptake of GnRH-III conjugate **10** (Dau) on MCF-7 breast cancer cells. Fluorescent pictures were taken using a confocal laser scanning microscope (after 5, 15, 30 and 60 s (left) as well as 5, 10, 30 and 60 min (right) incubation). DAPI (blue) and GnRH-III conjugate **10** (Dau, red) were excited at 405 and 458 nm respectively. Emission was collected at 450–510 nm for DAPI, 550–599 nm for GnRH-III conjugate 10 (DAU). The scale bar represents 10 μm.

It was also shown that their receptor binding affinity and degradation in lysosomes is similar, so it has no influence on biological activity (**Figure 4.**).
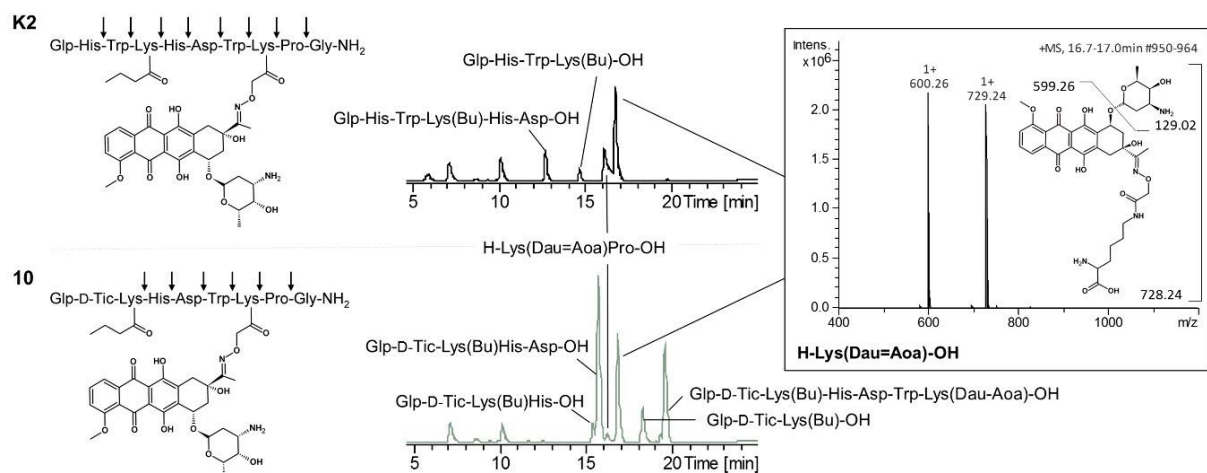

Figure 4. Degradation of the GnRH-III conjugates **K2** and **10** in presence of lysosomal rat liver homogenate. Cleavage sites produced by lysosomal enzymes are shown by full line arrows (left). LC chromatograms of **K2** and **10** after 24 h degradation (middle) and MS spectra of the active metabolite H-Lys(Dau=Aoa)-OH (right).

The antitumor activity of the previously developed GnRH-III-[^{4}Lys(Bu),^{8}Lys(Dau=Aoa)] conjugate (**K2**) and the novel synthesized GnRH-III-[$^2\Delta$His,^{3}D-Tic,4Lys(Bu),^{8}Lys(Dau=Aoa)] conjugate **10**, containing the anticancer drug daunorubicin, were further investigated on different tumor cells (breast, colon, lung, prostate, ovarian, pancreas, head and neck tumors, glioma an melanomas) [15]. It was indicated that both GnRH-III-Dau conjugates possess an efficient growth inhibitory effect on more than 20 cancer cell lines, whereby the biological activity is strongly connected to the expression of gonadotropin-releasing hormone receptors (GnRH-R). The novel conjugate showed a higher *in vitro* anti-proliferative activity and a higher uptake capacity. Moreover, the treatment with GnRH-III-Dau conjugates causes a significant *in vivo* tumor growth and metastases inhibitory effect in three different orthotopic models, including 4T1 mice and MDA-MB-231 human breast carcinoma, as well as HT-29 human colorectal cancer bearing Balb/c and SCID mice, while toxic side-effects were substantially reduced in comparison to the treatment with the free drug (**Figure 5.**) These findings illustrate that our novel lead compound is a highly promising candidate for targeted tumor therapy in both colon cancer and metastatic breast cancer.
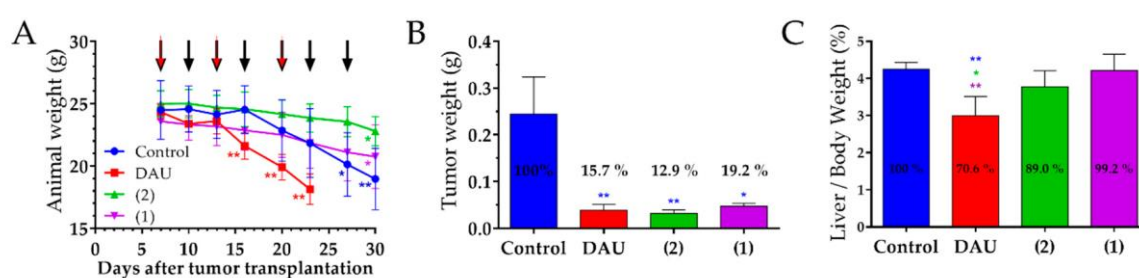
Figure 5. Effect of GnRH-III-Dau conjugates 1 (**K2**) and 2 (**10**) (10 mg/kg Dau content, 7 treatments, black arrows) and free Dau (1 mg/kg, 3 treatments, red arrows) in orthotopic HT-29 human colon carcinoma bearing mice. (A) Animal body weight (grams, average ± SD). (B) Tumor weight (grams, average ± SEM) of mice from control, Dau, 1 and 2 groups after termination of experiment, 30 days after transplantation. (C) Liver weight/body weight ratio (percentage, average ± SD) of mice from control, Dau, 1 and 2 groups after termination of the experiment, 30 days after transplantation. Tumor and liver weight of mice from free Dau group on day 23 subsequent to transplantation, 6 animals per group, statistical analysis was performed by Mann−Whitney test. * and ** mean significant at $p < 0.05$ and $p < 0.01$ respectively. * blue, red, purple, and green mean significant difference in control, Dau, 1, and 2 groups, respectively, at the end of experiment compared to the start (A), and significant difference compared to control, Dau, 1, and 2 groups respectively (B,C).

In case of breast MDA-MB-231 breast cancer, significant decrease of metastases was also observed. Numbers of mice with metastases were 5/5 (control group), 4/7 (Dau treated), 3/7 (**K2**), 3/7 (**10**). The above mentioned two GnRH derivatives were used for further studies to increase the antitumor effect of conjugates. Considering that the selective release of drugs in cancer cells is of high relevance, we were encouraged to develop cleavable, self-immolative GnRH-III-drug conjugates which consist of a *p*-aminobenzyloxycarbonlyl (PABC) spacer between a cathepsin B-cleavable dipeptide (Val-Ala, Val-Cit) and the classical anticancer drugs daunorubicin (Dau) and paclitaxel (PTX) (**Scheme 1.**) [16].
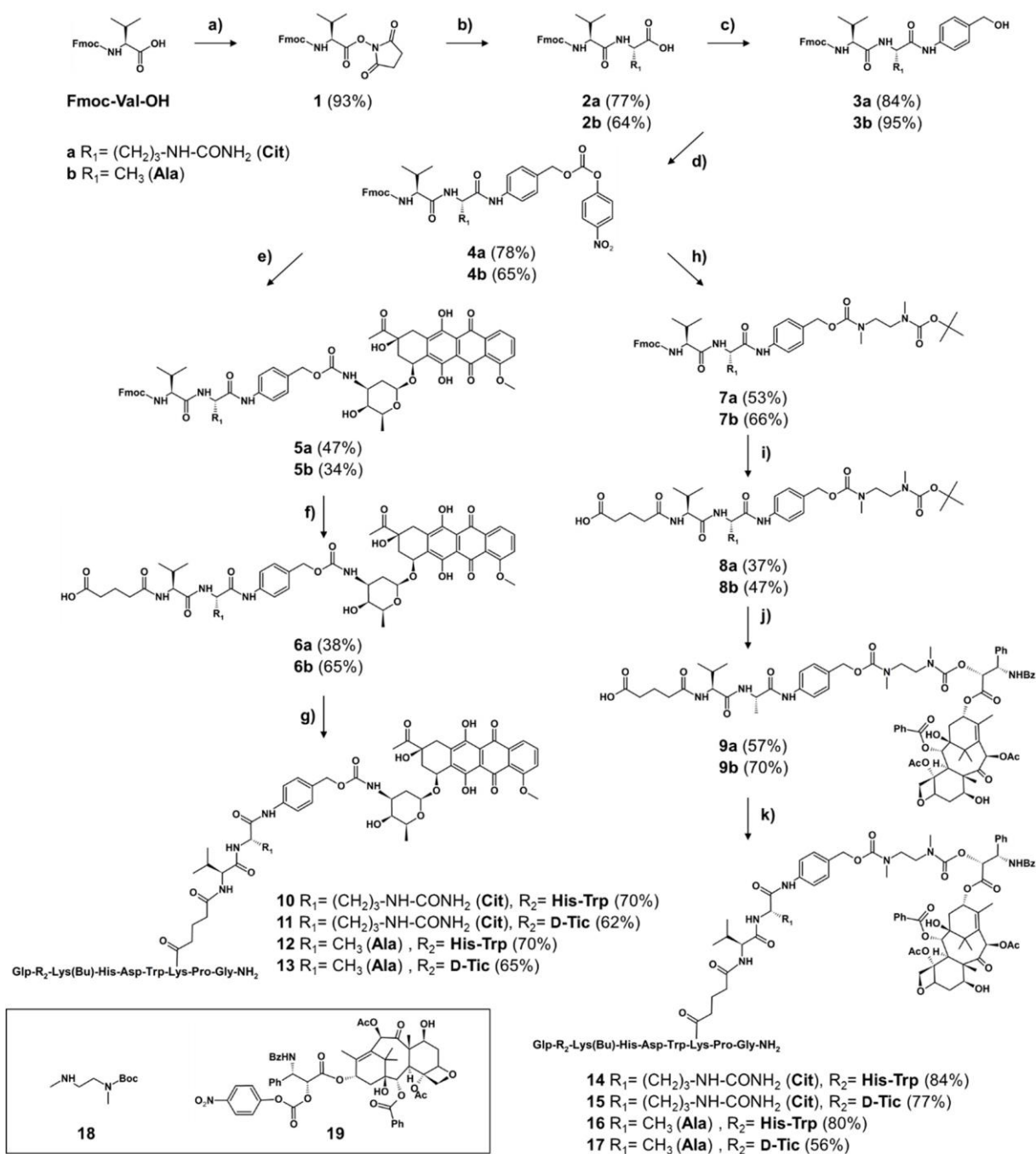
Scheme 1. Synthesis of self-immolative linker-containing GnRH-III-Dau and -PTX conjugates (a) 1 eq HOSu, 1 eq DCC in THF, overnight, RT, (b) 2a: 1.05 eq L-Cit-OH, 1.05 eq NaHCO$_3$ in H$_2$O/DME (1:1, v/v), overnight, RT, 2b: 1.1 eq L-Ala-OH, 1.1 eq NaHCO3 in H$_2$O/DME (3:2, v/v), overnight, RT, (c) 2 eq PAB-OH, 2 eq EEDQ in DCM/MeOH (2:1, v/v), overnight, RT, (d) 2 eq (Pnp)$_2$CO, 2eq DIPEA in DMF, overnight, RT, (e) 5a: 1 eq 4a, 1.1 eq Dau, 1.5 eq DIPEA in DMF, overnight, RT, 5b: 1.5 eq 4b, 1 eq Dau, 1.9 eq DIPEA in DMF, overnight, RT, (f) 1.) 5 eq piperidine in DMF, 2.) 2 eq glutaric anhydride, 2 eq DIPEA in DMF, 2 h, RT, (g) 1.) 1 eq 6a or 6b, 0.9 eq HATU, 2 eq DIPEA in DMF 30 min, 2.) 1 eq peptide I or II, overnight, RT, (h) 2.5 eq 18, 2.5 eq DIPEA in DMF, overnight, RT, (i) 1.) 5 eq piperidine in DMF, 2.) 2 eq glutaric anhydride, 2 eq DIPEA in DMF, overnight, RT, (j) 1.) TFA/DCM (1:2, v/v), 45 min, RT, 2.) 1.3 eq activated PTX (19), 4 eq DIPEA in DMF, overnight, RT, (k) 1.) 1 eq 9a or 9b, 0.9 eq HATU, 2 eq DIPEA in DMF 30 min, 2.) 1 eq peptide I or II, overnight, RT.

Alongside these compounds, non-cleavable GnRH-III-drug conjugates were also synthesized, and all compounds were analyzed for their antiproliferative activity. The cleavable GnRH-III bioconjugates

revealed a growth inhibitory effect on GnRH receptor-expressing A2780 ovarian cancer cells, while their activity was reduced (10 times lower) on Panc-1 pancreatic cancer cells exhibiting a lower GnRH receptor level. Moreover, the antiproliferative activity of the non-cleavable counterparts was strongly reduced. The PTX conjugates showed one order of magnitude higher antitumor activity (< 1 μM) than the Dau containing counterparts. Additionally, the efficient cleavage of the Val-Ala linker and the subsequent release of the drugs could be verified by lysosomal degradation studies (**Figure 6.**), while radioligand binding studies ensured that the GnRH-III-drug conjugates bound to the GnRH receptor with high affinity. Interestingly the Dau conjugates with self-immolative spacer did not show higher antitumor active than the oxime-linked versions (see above) that could be explained by the receptor binding affinity (3-10 times reduced affinity). The lower binding activity might be related to the bulkiness of the linker in comparison with oxime-linkage. Our results underline the high value of GnRH-III-based homing devices and the application of cathepsin B-cleavable linker systems for the development of small molecule drug conjugates (SMDCs).
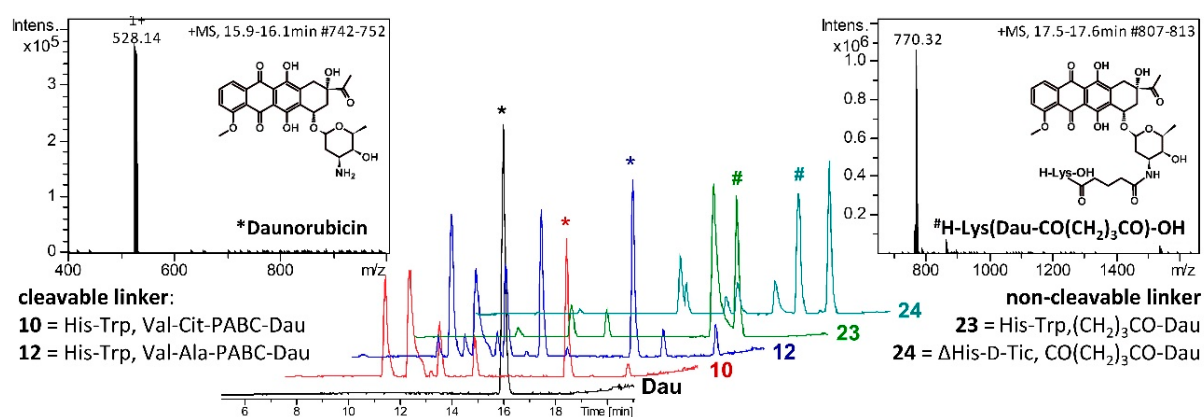

Figure 6. Degradation of the GnRH-III conjugates in presence of lysosomal rat liver homogenate. LC chromatograms of 10, 12, 23, 24 and free Dau (control) after 24 h degradation and MS spectra of the released * daunorubicin (left) and non-cleavable metabolite, # H-Lys(Dau-CO(CH$_2$)$_3$CO)-OH (right).

## 3. Suitability of GnRH receptors for targeted photodynamic therapy in head and neck cancers

Head and neck squamous cell carcinomas (HNSCC) have a high mortality rate, although several potential therapeutic targets have already been identified. Gonadotropin-releasing hormone receptor (GnRH-R) expression is less studied in head and neck cancers hence, we investigated the therapeutic relevance of GnRH-R targeting in HNSCC patients. Our results indicated that half of the patient-derived samples showed high GnRH-R expression, which was associated with worse prognosis, making this receptor a promising target for GnRH-based drug delivery [17]. Photodynamic therapy [18] is a clinically approved treatment for HNSCC, and the efficacy and selectivity may be enhanced by the covalent conjugation of the photosensitizer to a GnRH-R targeting peptide. Several native ligands, gonadotropin-releasing hormone (GnRH) isoforms, are known to target GnRH-R respectively. Therefore, different [4]Lys(Bu) modified GnRH analogs were designed and conjugated to protoporphyrin

IX (PpIX). The receptor binding potency of the novel conjugates was measured on human pituitary and human prostate cancer cells, indicating only slightly lower GnRH-R affinity than the peptides. The *in vitro* cell viability inhibition was tested on Detroit-562 human pharyngeal carcinoma cells that express GnRH-R in high levels (**Figure 7.**), and the results showed that all conjugates were more effective than the free PpIX (**Figure 8.**). The treatment schedules were also optimized (time of pretreatment and irradiation) [19].
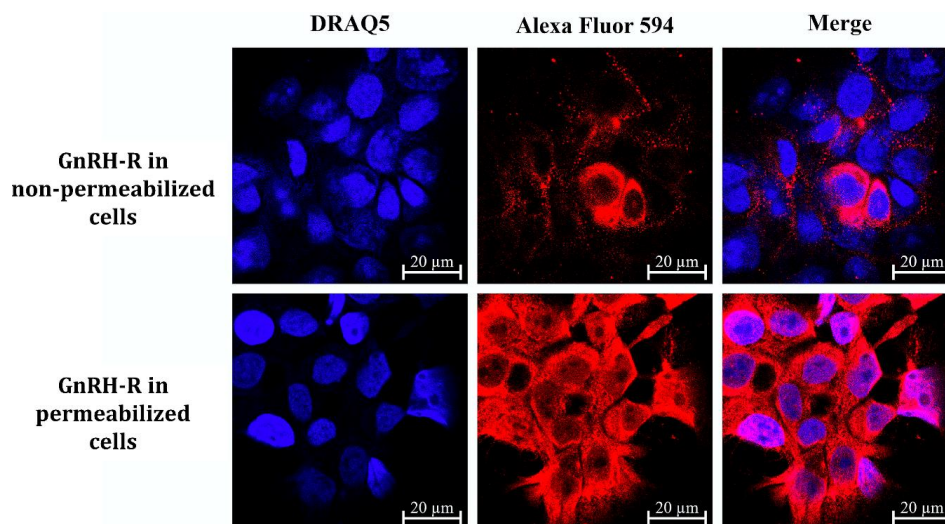
Figure 7. GnRH-R in Detroit-562 cells. The measurements confirm the high GnRH-R expression of Detroit-562 cells (GnRH-R in permeabilized cells) and the high number of receptors on non-permeabilized cells (nuclei: blue–DRAQ5; GnRH-R: red–Alexa Fluor 594).

The IC_{50} values (in nM) were 62.3 ±5.9 for GnRH-I[^{6}D-Lys(PpIX)] (**5**), 89.8±19.2 for GnRH-I[^{4}Lys(Bu), ^{6}D-Lys(PpIX)] (**6**), 71.1±6.2 for GnRH-II[^{4}Lys(Bu), ^{6}D-Lys(PpIX)] (**7**), 81.8±12.6 for GnRH-III[^{4}Lys(Bu), ^{6}Asp(OMe), ^{8}D-Lys(PpIX)] (**8**), and for PpIX 209±119.5, respectively.
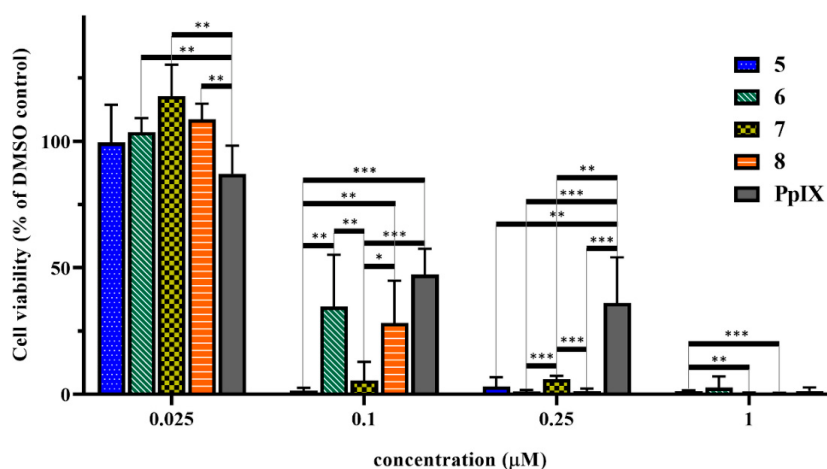
Figure 8. *In vitro* cell viability inhibition effect of the prepared GnRH-PpIX conjugates (compounds **5–8**) and PpIX using 5 h incubation and a 10 min irradiation period. Cell viability values are present in % of DMSO control. ($* p < 0.05$; $** p < 0.01$; $*** p < 0.001$).

4. Cardiotoxicity studies of GnRH derivative – drug conjugates.

Cardiomyopathy induced by the chemotherapeutic agent doxorubicin and daunorubicin is a major limiting factor for their application in cancer therapy [20]. The attachment of the aforementioned chemotherapeutic drugs to GnRH-based peptides may result in compounds with decreased toxic side effect. The objective of our study was to examine the cytotoxic effect of anticancer drug–GnRH-conjugates against two essential cardiovascular cell types, such as cardiomyocytes and endothelial cells. Sixteen different previously developed GnRH-conjugates containing doxorubicin, daunorubicin and methotrexate were investigated in this study. Their cytotoxicity was determined on primary human cardiac myocytes (HCM) and human umbilical vein endothelial cells (HUVEC) using the xCELLigence SP system, which measures impedance changes caused by adhering cells on golden electrode arrays placed at the bottom of the wells. Slopes of impedance–time curves were calculated and for the quantitative determination of cytotoxicity, the difference to the control was analyzed.

The results indicated that the oxime-linked Dau-peptide conjugates had no or only a mild cardiotoxicity in comparison with the free anthracycline drug molecules (**Figure 9.**). However, in the case of the conjugate AN-152, in which doxorubicin is attached to GnRH-I derivative through an ester bond, showed significant toxicity [21]. This conjugate is in Phase-III Clinical Trial (Zoptarelin doxorubicin), and this side effect can be explained by the low serum stability of the ester bond between the drug molecule and homing peptide resulting in early drug release before reaching the target cells.

5. Comparison of apoptotic effect and antimetastatic effect of GnRH derivative – drug conjugates

We demonstrated that the modification with Lys(Bu) (Bu is butyryl moiety) in position 4 resulted in an increase in the cytotoxic and apoptotic effect and the internalization ability of GnRH-I and GnRH-III conjugates containing an oxime-linked Dau [22]. Although the conjugates had a minor apoptotic effect, they could regulate the expression of several apoptosis-related factors, and this activity proved to be sensitive to the GnRH isoforms and the presence of the ^{4}Lys(Bu), especially in the case of TNF, TP53 and members of the growth-factor signaling pathway. By detecting the expression of 23 apoptosis related genes, we could find further evidence that the GnRH-I and GnRH-III conjugates acted in a more or less similar way. Our comprehensive PCR results show that the stronger cytotoxic activity of I-[^{4}Lys(Bu),^{6}D-Lys(Dau)], III-[^{4}Lys(Bu),^{8}Lys(Dau)] and II-[^{4}Ser,^{6}D-Lys(Dau)] was associated with a stronger and a more immediate inhibitory effect on the expression of the elements of growth-factor signaling compared to their counterparts, where the upregulation of the expression of TP53, TNF and caspases (*e.g.,* CASP9) probably had a more important role. Our results also suggest the significance of ^{4}Lys(Bu) in the receptor binding or activation of GnRH-I and GnRH-III conjugates, while in the case of GnRH-II conjugates, the native Ser in position 4 appeared to be more important. We were able to provide further evidence that targeting the GnRH-R could serve as a successful therapeutic approach in colon cancer, and III-[^{4}Lys(Bu),^{8}Lys(Dau)] was proven to be the best candidate for this purpose [23].
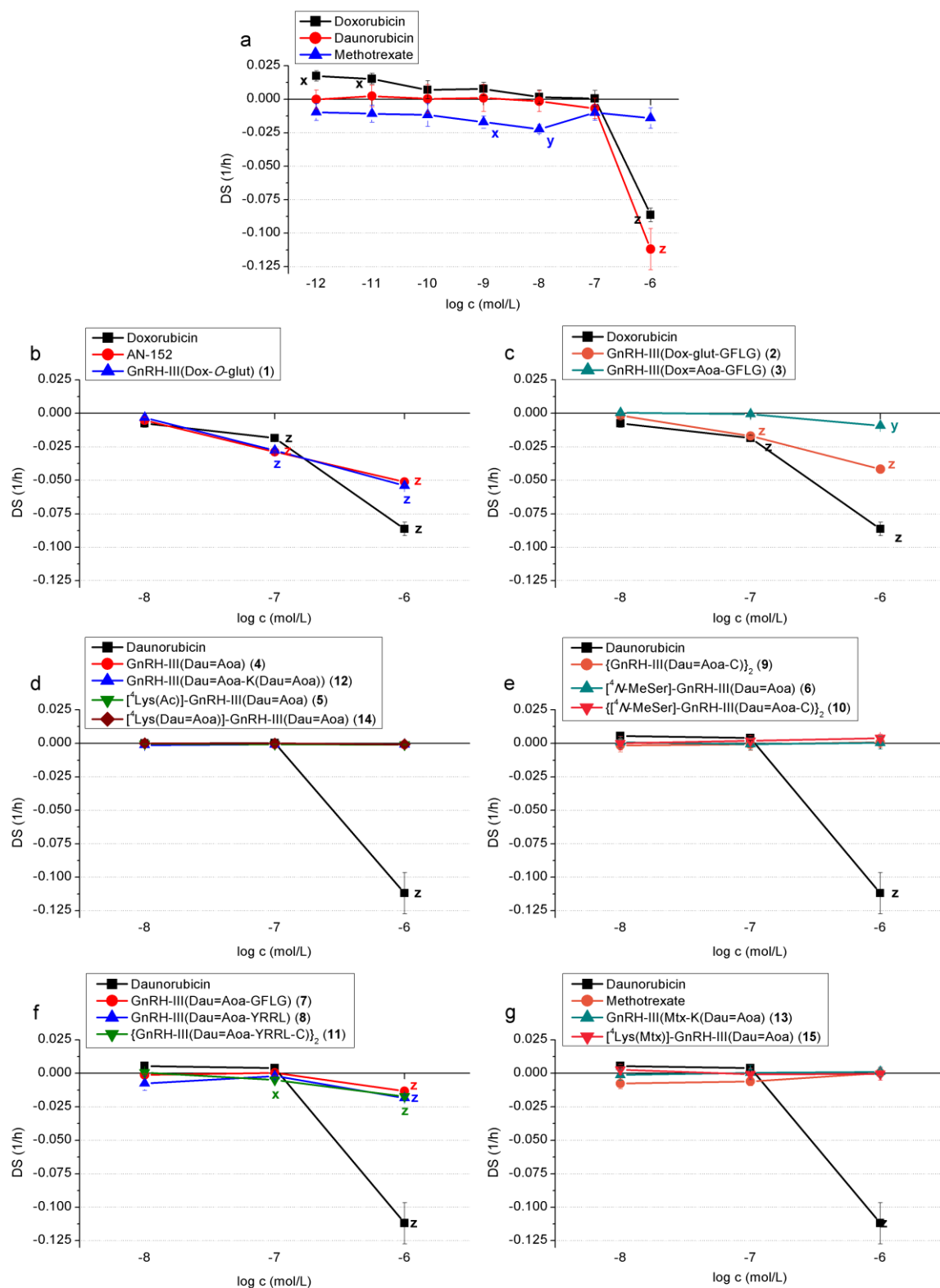
Figure 9. Long-term cytotoxic effects – impedimetrically registered negative effect on cell proliferation/viability – of chemotherapeutic drugs (doxorubicin, daunorubicin, methotrexate) and their GnRH-III conjugates on HUVEC cells. (a) Chemotherapeutic drugs (doxorubicin, daunorubicin, methotrexate);(b) GnRH conjugates containing doxorubicin without spacer sequence; (c) with spacer sequence GFLG; (d) oxime bond-linked, mono- and bifunctional daunorubicin-GnRH-III conjugates without spacer and modified in position 4 with Lys; (e) {GnRH-III(Dau=Aoa-C)}₂ dimer and conjugates modified in position 4 with *N*-MeSer; (f) GFLG or YRRL spacer containing monomer and dimer conjugates (g) GnRH-III conjugates containing methotrexate and daunorubicin.

Our findings also suggested that the underlying mechanisms of their antitumor effects, as well as their adhesion modulator and chemotactic/chemokinetic activities depends on the length of the side chain in [4]Lys. It was clearly shown that [[4]Lys(Bu)]-GnRH-III(Dau=Aoa) possessing a longer, butyryl side chain could reduce the cell viability through its pro-apoptotic effect and the migratory/chemotactic behavior of melanoma cells, as well. Whereas, [[4]Lys(Ac)]-GnRH-III(Dau=Aoa) was appeared to elicit its antitumor effect by arresting the cell cycle in G2/M phase and enhanced the migratory responses of melanoma cells. Our findings indicate the possibility that the locomotory reaction of melanoma cells induced by [[4]Lys(Bu)]-GnRH-III(Dau=Aoa) and GnRH-III(Dau=Aoa) could be associated with the cell adhesion and morphological changes induced by these conjugates. Based on the overall cell biological effects of [[4]Lys(Bu)]-GnRH-III(Dau=Aoa), the presence of butyrate-containing Lys could provide benefits over the conjugates possessing Lys(Ac) or Ser in position 4. Our results, together with previous data, would suggest the idea that the butyrate could work as a "second drug" in the conjugate. On the basis of the combined cytotoxic, adhesion inducer and cell movement inhibitory effect, [[4]Lys(Bu)]-GnRH-III(Dau=Aoa) proved to be the best candidate in our study for application in the targeted melanoma therapy as a multifunctional antitumor and antimetastatic drug delivery system [24].

6. Neurotensin-based drug conjugates for the treatment of pancreatic ductal adenocarcinoma

At present days, Pancreatic Ductal Adenocarcinoma (PDAC) is one of the most aggressive and dangerous cancerous diseases with a high mortality rate [25]. Only in the USA, approximately 56000 new cases were diagnosed followed by death of 45000 patients within a year, furthermore the estimated data in the following years show increment of the number of new cases and deaths. PDAC is only 3-4% of all newly diagnosed cancer cases but the mortality of this malignancy is more than 80% [26]. The average 5-years survival rate is approximately 10% [27], because more than 80% of the patients are diagnosed with metastatic or inoperable status. The main reason for the high mortality of pancreatic cancer patients could be the very poor prognosis, because of the early diagnosis of PDAC is still difficult [28].

Neurotensin is a 13 amino acid containing gut-brain peptide hormone (neurotransmitter peptide) in the central nervous system, and in the gastrointestinal tract [29]. It shows complex physiological roles in central and peripheral administration, e.g. it is involved in the dopaminergic system. The investigation of structure-activity relationships suggested that carboxyl terminal end ([8]RRPYIL[13]) of the sequence contained the biological activity of this peptide [30]. Neurotensin is a growth factor in both normal and cancerous cells [31]. The role of the neurotensin/neurotensin receptor (NTS/NTSr) system was also described in the case of different types of cancer such as breast, lung, prostate, colorectal and pancreatic cancers [32]. It was indicated that more than 78% of PDAC cells are NTSr1 positive in contrast to other type of pancreatic tissues (healthy, chronic pancreatitis) which presents less than 35% NTSr1 positive cells.

Neurotensin-based Dau conjugates were designed based on the NTS[8-13] and NTS[6-13] sequences applying various structures with or without GFLG cathepsin B cleavable spacer (conjugates **1-6**) [33]. The peptides were synthesized with free carboxyl group at the C-terminus according to the native hormone peptide. The *in vitro* cytotoxicity studies indicated that the most effective conjugate was Dau=Aoa-KRRPYIL-OH (**2**) in which the RRPLYIL neurotensin fragment was elongated by a Lys at the N-terminus. The cell viability was 4.7 ± 1.78 (%) at treatment with 10^{-5} M concentration of the conjugate. The incorporation of GFLG spacer increased the cellular uptake, but not the antitumor effect that could be explained by the speed of the release of Dau containing metabolite. The *in vivo* experiments also suggested that conjugate **2** is the most potent in tumor growth inhibition (>30%) in case of Panc-1 tumor bearing mice without significant toxic side effect (**Figure 10.**). In contrast, the free Dau showed significant toxicity at maximum tolerated dose (1 mg/kg) therefore, the mice in Dau treated group had to terminated on the day 63, while the experiment was finished on day 86 in other groups. It worth mentioning that the free peptide alone significantly increased the tumor growth by 35.1%.
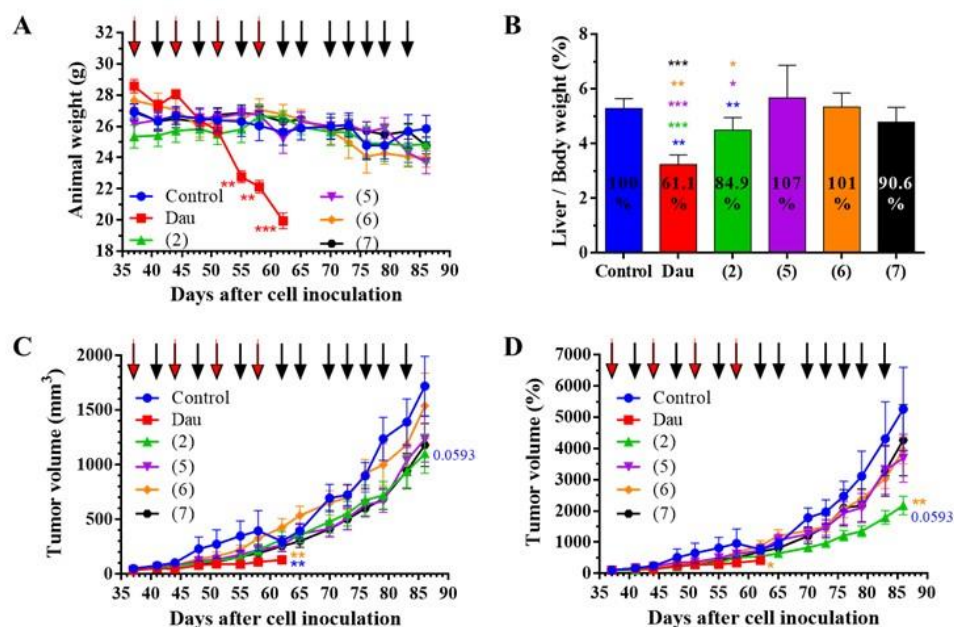
Figure 10. Effect of Dau-conjugates **2**, **5**, **6** and **7** (5 mg/kg Dau content, 14 treatments, black arrows) and free Dau (1 mg/kg, 4 treatments, red arrows) in subcutaneous Panc-1 human pancreatic cancer bearing SCID female mice. (A) Animal body weight (grams, average ± SEM). (B) Liver weight/body weight ratio (percentage, average ± SD) after termination of experiment, 86 days subsequent to cells inoculation for conjugates, and 62 days for Dau treated group. (C) Tumor volume (mm3, average ± SEM). (D) Tumor volume (percentage, average ± SEM). Statistical analysis was performed by Mann–Whitney test. *, ** and *** mean significant at $p \le 0.05$, $p \le 0.01$ and $p \le 0.001$, respectively. * red means significant difference in Dau group at certain time point of experiment compared to the start (A). * blue, green, purple, orange and black mean significant difference compared to the control, 2, 5, 6 and 7 groups respectively (B, C, D).

7. Bombesin derivatives for efficient drug targeting

Our research group also have focused on the Gastrin Releasing Peptide Receptor (GRP-R, or Bombesin Receptor 2, BB2), which is overexpressed in several malignancies, such as prostate, breast and lung cancer, while being poorly expressed physiologically in healthy tissues [34]. This receptor is part of the bombesin receptors family together with the Neuromedin B receptor (NMB-R, BB1) and the Bombesin Receptor Subtype 3 (BRS-3, BB3). Its native ligand, the Gastrin-Releasing Peptide, of which the C-terminal heptapeptide fragment is common with Bombesin (BBN), a 14-mer amino-acid peptide, was first discovered in the skin of the European fire-bellied toad, *Bombina bombina* [35]. The mentioned truncated version, BBN(7-14) (Gln-Trp-Ala-Val-Gly-His-Leu-Met-NH$_2$), maintains the affinity towards GRP-R. From this sequence, several modified peptides were developed to increase their receptor binding affinity and plasma stability [36,37], but also with modulated agonist or antagonist activity [38]. However, these peptides were not compared as tumor homing peptides for drug targeting. Therefore, our goal was to prepare Dau conjugates from these bombesin analogs and compare their antitumor activity *in vitro* and *in vivo*. In addition, we developed a new bombesin analog with four substitution (**D-Phe**-Gln-Trp-Ala-Val-**βAla**-His-**Sta**-**Nle**-NH$_2$) and it was investigated for drug delivery [39]. Dau was attached to the peptide through GFLG or LRRY Cathepsin B cleavable spacers via oxime linkage. However, the conjugates with GFLG spacer had pure solubility, therefore, LRRY spacer was applied further. Three conjugates showed promising *in vitro* cytostatic effect at low micromolar concentration (Dau=Aoa-LRRY-QWAVGHLNle-NH$_2$ (**L1**) and cellular uptake by breast and prostate tumors (Dau=Aoa-LRRY-fQWAVGHStaL-NH$_2$ (**L5**), and (Dau=Aoa-LRRY-fQWAV-βAla-H-Sta-Nle-NH$_2$ (**L6**), where f is D-Phe, Sta is statine and Nle is norleucine) (**Table 1**. and **Table 2**.). The first one showed very low plasma stability therefore, the two others were investigated for *in vivo* experiments (**Figure 11**.)
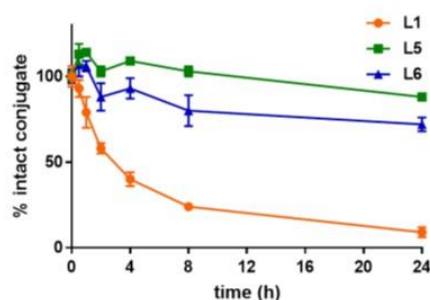
Figure 11. Stability of compounds **L1**, **L5** and **L6** in mouse plasma over 24 h. **L5** and **L6** clearly show a more promising profile than **L1.** Moreover, despite **L1** still has an acceptable half-life of 3.8 h, the release of Dau=Aoa-Leu-OH is detected after 2 h. The percentage of intact conjugate at each time point is the mean ± SD of three replicates.

Table 1. IC_{50} values related to the cytostatic effect of the Dau-BBN(7-14) conjugates and the free peptides on human breast cancer MDA-MB-231 and MDA-MB-453 and human prostate cancer PC-3 cell lines. All values are reported as mean ± SD.

Conjugate / free peptide	MDA-MB-231 IC_{50} (μM)	MDA-MB-453 IC_{50} (μM)	PC-3 IC_{50} (μM)
G1	22.80 ± 3.12	11.45 ± 1.53	11.83 ± 2.50
G2	7.29 ± 3.41	12.72 ± 1.22	5.98 ± 2.10
G3	9.28 ± 0.13	8.78 ± 0.97	4.55 ± 0.76
G4	20.98 ± 0.55	7.37 ± 1.28	5.73 ± 0.24
G5	18.29 ± 1.46	11.62 ± 3.33	9.69 ± 0.17
G6	9.16 ± 1.27	16.11 ± 5.06	7.48 ± 1.03
L1	4.15 ± 0.18	7.87 ± 0.09	4.38 ± 0.33
L2	11.74 ± 0.09	19.14 ± 0.49	8.57 ± 1.61
L3	18.96 ± 3.23	>25	>25
L4	5.31 ± 0.01	21.21 ± 5.36	4.08 ± 0.09
L5	3.35 ± 0.32	5.86 ± 0.75	2.22 ± 0.19
L6	9.88 ± 2.82	9.64 ± 0.25	18.04 ± 3.01
FP1	>100	>100	>100
FP2	>100	>100	>100
Dau	0.90 ± 0.06	0.81 ± 0.07	0.75 ± 0.01

Table 2. UC_{50} values related to the uptake of the conjugates in the indicated human cancer cell lines after 1.5 h incubation. Each value indicates the concentration (μM) that corresponds to the internalization of 50% of the conjugate inside the cells.

Conjugate / free peptide	MDA-MB-231 UC_{50} (μM)	MDA-MB-453 UC_{50} (μM)	PC-3 UC_{50} (μM)
G1	>25	>25	>25
G2	>25	17.04	10.50
G3	>25	22.59	>25
G4	23.33	20.22	>25
G5	>25	>25	>25
G6	>25	>25	>25
L1	18.67	11.63	22.92
L2	18.27	21.58	20.87
L3	>25	24.59	>25
L4	>25	>25	>25
L5	15.87	8.96	12.35
L6	15.47	4.15	16.09

In *in vivo* experiments on PC-3 prostate cancer, compounds **L5** and **L6** showed significantly lower toxicity compared to free daunorubicin, even though the conjugates were applied in a much higher dose, 10 mg Dau content in conjugates/kg in comparison with 1 mg/kg dose of Dau as MTD. The animals treated with free Dau had to be terminated on day 26, because of the toxicity of the drug resulted in significant weight loss of mice. In the case of conjugate-treated mice, the size of the tumors was not significantly smaller at the termination of the experiment compared to controls; however, **L5** and **L6**

treatments resulted in 21.4% and 31.4% growth inhibition, respectively. When comparing tumor weights, **L5**-treated mice showed a decrease of 16.6%, whereas **L6**-treated mice exhibited 33.1% reduction compared to control animals at day 33 (**Figure 12.**).
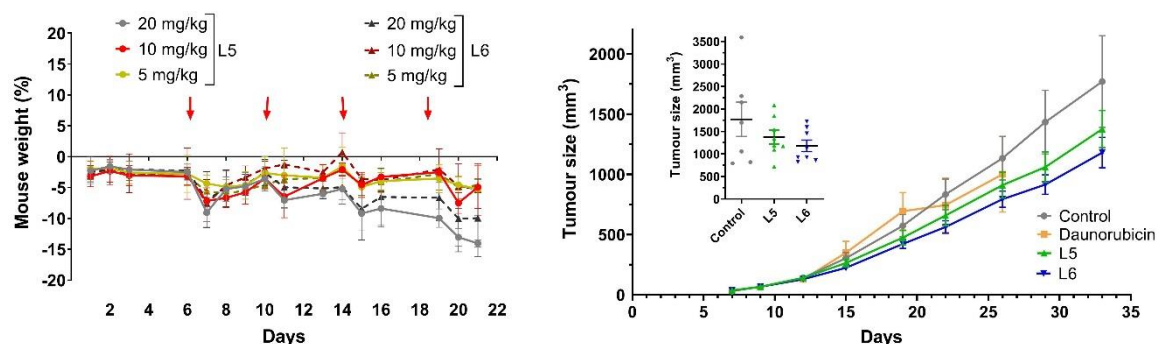

Figure 12. *In vivo* toxicity and antitumor effect of conjugates **L5** and **L6**. (A) Mouse body weight (%, mean ± SD) after administration of either **L5** and **L6**, in three different concentrations, calculated on Dau content: 5 mg/kg, 10 mg/kg and 20 mg/kg. Four treatments (red arrows), three mice per group. (B) Tumor volume (mm³, mean ± SEM). Administration regime: 0.9% saline, (control group), Dau (1 mg/kg) and conjugates (10 mg/kg calculated on Dau content), every 5th day.

The obtained results suggested that the conjugate with new bombesin analog as homing peptide developed in our laboratory (**L6**) might be a good candidate for drug targeting through bombesin receptor-2 (BB2-R or GRP-R).

8. Application of cyclic NGR peptides for drug delivery

Peptides containing the asparagine-glycine-arginine (NGR) motif are recognized by CD13/aminopeptidase N (APN) receptor isoforms that are selectively overexpressed in tumor neovasculature [40]. Spontaneous decomposition of NGR peptides can result in *iso*Asp derivatives, which are recognized by RGD-binding integrins that are essential for tumor metastasis [41]. Peptides binding to CD13 and RGD-binding integrins provide tumor-homing, which can be exploited for dual targeted delivery of anticancer drugs. Therefore, we synthesized small cyclic NGR peptide–daunomycin conjugates using NGR peptides of varying stability (c[KNGRE]-NH$_2$, Ac-c[CNGRC]-NH$_2$ and the thioether bond containing c[CH$_2$-CO-NGRC]-NH$_2$, c[CH$_2$-COKNGRC]-NH$_2$) (**Figure 13.**)[42]. The cytotoxic effect of the novel cyclic NGR peptide-Dau conjugates were examined *in vitro* on CD13 positive HT-1080 (human fibrosarcoma) and CD13 negative HT29 (human colon adenocarcinoma) cell lines. Our results confirmed the influence of structure on the antitumor activity and dual acting properties of the conjugates. Attachment of the drug through an enzyme-labile spacer to the C-terminus of cyclic NGR peptide resulted in higher antitumor activity on both CD13 positive and negative cells as compared to the branching versions.
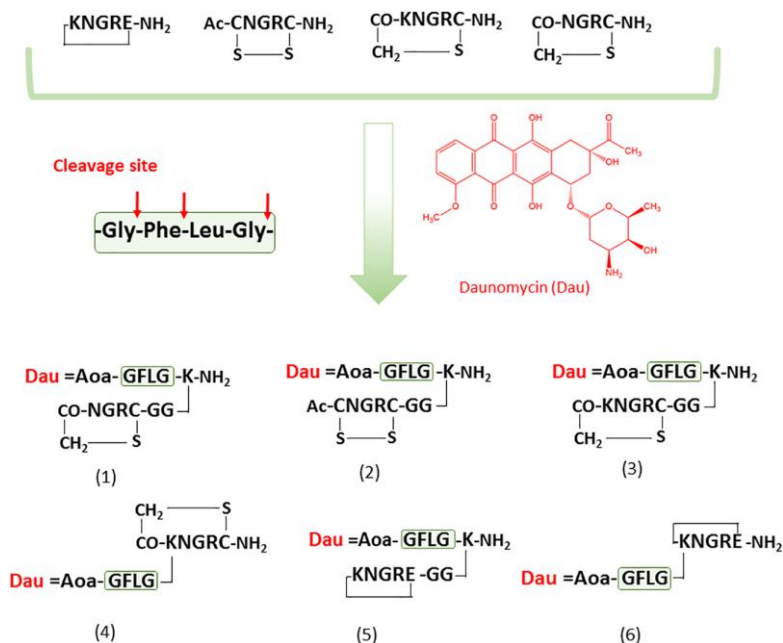
Figure 13. Structure of the cyclic NGR peptides and their Dau conjugates

Six new cyclic NGR peptide-daunomycin conjugates were prepared with different structure in terms of conjugation sites and applied linkage in the cycle. Chemostability (deamidation of Asn) of the conjugates and the free cyclic peptides [43] was found to be different. However, in most cases no correlation between the chemostability and selectivity or dual acting effect of conjugates could be identified. Therefore, further experiments are needed to analyze the binding affinity of conjugates to different receptors. Nevertheless, we can conclude that the conjugates in which the drug molecule is attached through C-terminal elongation of cyclic NGR peptides (conjugates **2**, **3**, **5**) have higher antitumor activity against both cell lines, irrespectively of the bond in the cycle, as compared to branched conjugates **4** and **6**. Conjugates **4** and **6** showed higher selectivity to HT-1080 cells. Therefore, conjugates **2**, **3** and **5** are suitable for dual targeting while conjugates **4** and **6** can be used for selective CD13 targeting. We also found that the antitumor activity of the NGR peptide-drug conjugates (**Table 4.**) depends not only on NGR-i*so*DGR rearrangement (**Table 5.**) but also on other complex mechanisms including enzyme degradation (**Figure 14.**), cellular uptake (**Figure 15**), and. In addition, conjugates **2**, **3** and **5** showed similar antitumor activity against HT-29 cells *in vitro* as the previously prepared GnRH-III-Dau conjugate [22] that had significant and better *in vivo* tumor growth inhibition effect compared to the free drug [44]. These results warrant the study of the *in vivo* antitumor effect of the most active NGR-Dau conjugates alone, or in combination with the GnRH-drug conjugate.

Table 4. Cytostatic/cytotoxic effect of cyclic NGR peptide±daunomycin conjugates.

| Code	Compounds	IC$_{50}$ (µM), 6 h[a]			IC$_{50}$ (µM), 72 h[b]		
		HT 1080	HT-29	p	HT 1080	HT-29	p
	Daunomycin	0.7±0.3	0.7±0.3	ns.	0.23±0.1	0.15±0.1	ns.
1	Dau =Aoa-GFLGK-NH$_2$ CH$_2$CO-NGRC-GG┘	≫50	≫50	ns.	23.8 ±0.7	20.6±5.6	ns.
2	Dau =Aoa-GFLGK-NH$_2$ Ac-CNGRC-GG┘	6.8±0.7	19.0±1.4	p < 0.01	2.0±0.3	3.3±0.9	ns.
3	Dau =Aoa-GFLGK-NH$_2$ CH$_2$CO-KNGRC-GG┘	8.0 ±0.1	10.3±2.2	ns.	3.3±0.6	5.7±0.9	ns.
4	CH$_2$CO-KNGRC-NH$_2$ Dau =Aoa-GFLG┘	45.2±13.2	≫50	ns.	14.5±2.0	≫50	p < 0.01
5	Dau =Aoa-GFLGK-NH$_2$ KNGRE-GG┘	5.7±0.5	8.7±1.2	ns.	1.4±0.1	3.0±0.6	p < 0.05
6	KNGRE-NH$_2$ Dau =Aoa-GFLG┘	43.7±4.1	≫50	ns.	15.8±4.4	≫50	p < 0.01

[a]Tests were carried out 4 times; [b]tests were carried out 3 times; IC$_{50}$ values were averaged; statistical significance was calculated using unpaired t-tests.

Table 5. Chemostability of cyclic NGR peptide-daunomycin conjugates

Code	Conjugates	ratio of Asn-/*iso*Asp-/Asp-containing peptide-drug conjugates (DMEM CM, 37°C)	
		6h	72h
1	Dau =Aoa-GFLGK-NH$_2$ CH$_2$CO-NGRC-GG┘	0/83/17	0/83/17
2	Dau =Aoa-GFLGK-NH$_2$ Ac-CNGRC-GG┘	100/0/0	74/0/26
3	Dau =Aoa-GFLGK-NH$_2$ CH$_2$CO-KNGRC-GG┘	0/57/43	0/57/43
4	CH$_2$CO-KNGRC-NH$_2$ Dau =Aoa-GFLG┘	30/48/22	0/62/38
5	Dau =Aoa-GFLGK-NH$_2$ KNGRE-GG┘	100/0/0	100/0/0
6	KNGRE-NH$_2$ Dau =Aoa-GFLG┘	100/0/0	54/0/46
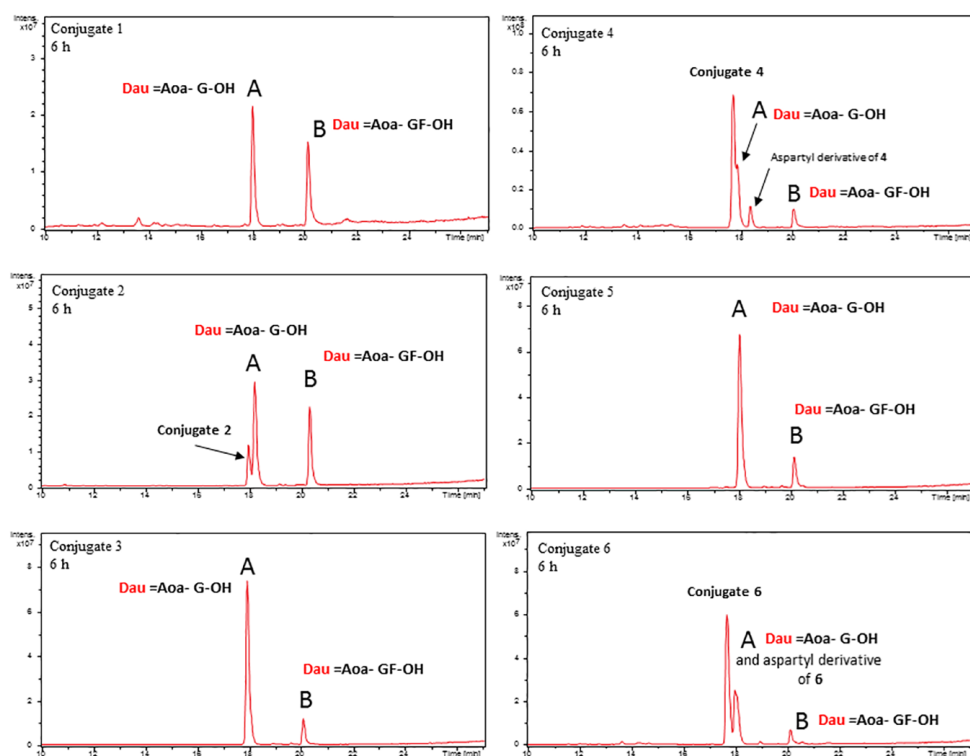
Figure 14. Lysosomal degradation of daunomycin-conjugates after 6 h
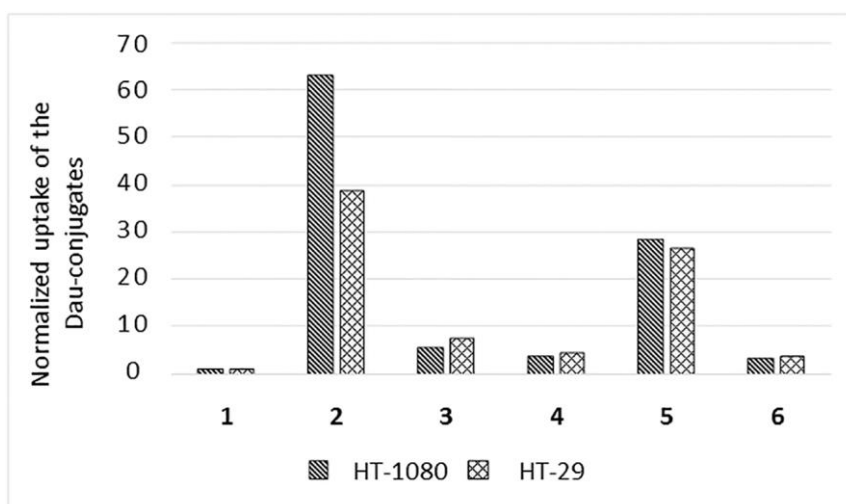
Figure 15. Direct uptake of daunomycin-conjugates. Normalized uptake values indicate the fold increase of the measured fluorescent units compared to the autofluorescence of empty cells.

In the above-mentioned study, it was indicated that the Dau=Aoa-GFLGK(c[KNGRE]-GG-)-NH$_2$ conjugate (**5**, but in this experiment, it is signed by **K**), which is stable against rearrangement but cleavable by Cathepsin B easily, has a significant antitumor activity against both CD13+ HT-1080 human fibrosarcoma and CD13− but integrin positive HT-29 human colon adenocarcinoma cells. Therefore, we used this compound for further studies. However, it seems that the free ε-amino group of Lys in the cycle is not necessary for the biological activity. Therefore, we developed novel cyclic NGR peptide–daunomycin conjugates in which Lys was replaced by different amino acids (Ala, Leu, Nle,

Pro, Ser) [45]. The exchange of the Lys residue in the cycle simplified the cyclization step and resulted in a higher yield. The new conjugates showed lower chemostability against deamidation of Asn than the control compound, thus they had lower selectivity to CD13+ cells (**Table 6.**). However, the cellular uptake and cytotoxic effect of Dau=Aoa-GFLGK(c[NleNGRE]-GG-)-NH$_2$ was higher in comparison to the control especially on HT-29 cells (**Table 7**. and **Figure 16**.).

Table 6. Chemostability of cyclic NGR peptide-Daunomycin conjugates

Code	AAA in position X of the conjugates	Ratio of Asn-/Asp-/isoAsp-derivatives (DMEM CM, 37 °C)	
		6 h NGR : DGR : *iso*DGR	72 h NGR : DGR : *iso*DGR
1	Ala	96 : 0 : 4	58 : 11 : 31
2	Leu	93 : 0 : 7	54 : 11 : 35
3	Nle	93 : 1 : 6	58 : 9 : 33
4	Pro	73 : 14 : 13	19 : 46 : 35
5	Ser	93 : 0 : 7	56 : 12 : 31
K	Lys	100 : 0 : 0	100 :0 : 0

Table 7. In vitro cytostatic/cytotoxic effects of compounds on HT-29 and HT-1080 cells

| Compounds	IC$_{50}$ (6 h) HT-1080	IC$_{50}$ (6 h) HT-29	IC$_{50}$ (72 h) HT-1080	IC$_{50}$ (72 h) HT-29
Daunomycin	1.4 ± 0.6	0.3 ± 0.2	0.5 ± 0.2	0.1 ± 0.1
Dau=Aoa-GFLGK(c[KNGRE]-GG)-NH$_2$ (**K**)	5.7 ± 0.5	8.7 ± 1.2	1.4 ± 0.7	3.0 ± 0.6
Dau=Aoa-GFLGK(c[ANGRE]-GG)-NH$_2$ (**1**)	8.9 ± 0.8	4.3 ± 0.5	3.6 ± 0.7	3.2 ± 0.8
Dau=Aoa-GFLGK(c[LNGRE]-GG)-NH$_2$ (**2**)	57.5 ± 6.3	47.0 ± 5.4	20.6 ± 0.4	14.1 ± 0.7
Dau=Aoa-GFLGK(c[NleNGRE]-GG)-NH$_2$ (**3**)	5.5 ± 0.3	2.2 ± 0.2	2.3 ± 0.6	1.3 ± 0.2
Dau=Aoa-GFLGK(c[PNGRE]-GG)-NH$_2$ (**4**)	9.4 ± 4.0	14.6 ± 4.7	3.5 ±1.0	3.7 ± 0.8
Dau=Aoa-GFLGK(c[SNGRE]-GG)-NH$_2$ (**5**)	>100	64.7 ± 4.9	63.7 ± 9.5	39.4 ± 2.9
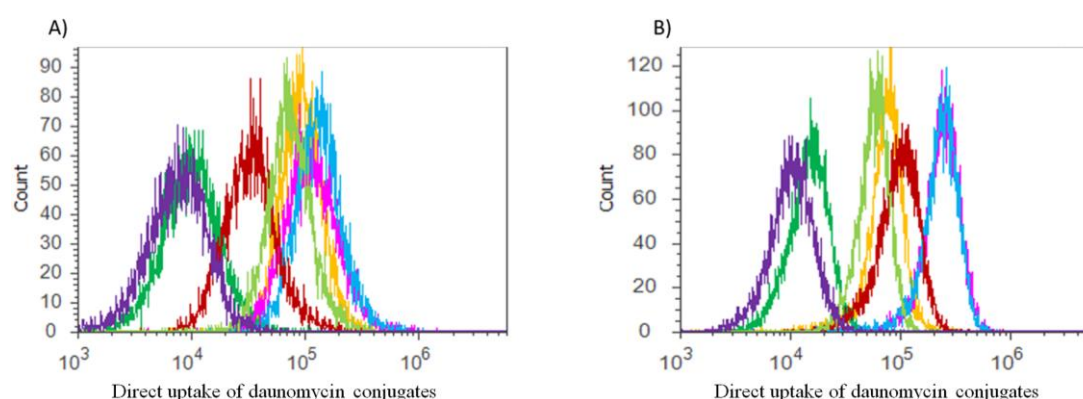
Figure 16. (A) HT1080 and (B) HT-29 cells. Uptake of conjugate **1** (light green); **2** (red); **3** (light blue); **4** (pink); **5** (green); **K** (yellow). Empty control with purple color.

From this study we can conclude that replacement of Lys in the Dau=Aoa-GFLGK(c[KNGRE]-GG)-NH$_2$ conjugate by different amino acids provides a more convenient and cost-effective synthetic route resulting in a higher yield, which might be relevant for larger scale synthesis needed for further *in vivo* studies. We show that the changes decrease the chemostability of the cyclic NGR moiety, resulting in

the formation of *iso*Asp derivatives in higher amount. Among the new cyclic NGR peptide–daunomycin conjugates the most effective compound was Dau=Aoa-GFLGK(c[NleNGRE]-GG)-NH$_2$, which showed similar activity against HT-1080 CD13+ cells to Dau=Aoa-GFLGK(c[KNGRE]-GG)-NH$_2$, and a significantly higher antitumor effect against HT-29 CD13− but integrin receptor positive cells. This might be explained by the binding affinity of *iso*DGR peptides to integrin receptors. However, to confirm these findings further binding studies of cyclic NGR peptide–drug conjugates to different integrin receptors are needed. Taken together, the synthetic and biological results suggest that the Dau=Aoa-GFLGK(c[NleNGRE]-GG)-NH$_2$ conjugate is more suitable for drug targeting with dual acting propensity than our control lead compound.

Because HT1080 cannot be used in *in vivo* experiments Kaposi sarcoma (KS) bearing mice were involved in this experiment. It was indicated that KS cells express CD13 on their suface in much higher amount than HT-29 colon carcinoma cells (**Figure 17**) [46].
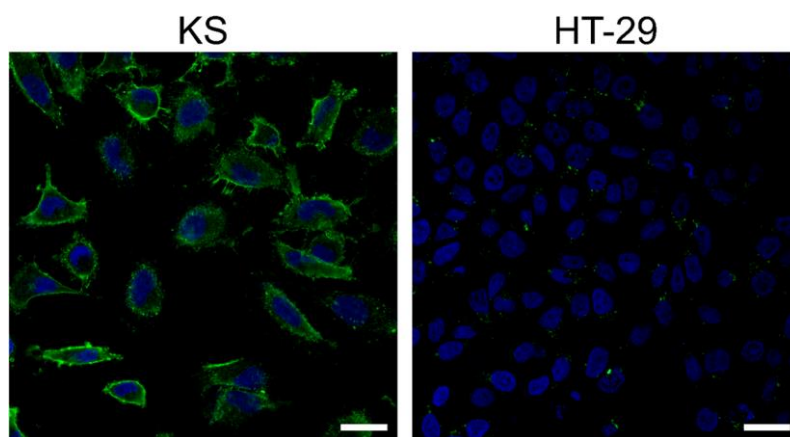

Figure 17. Determination of cell surface CD13 expression on KS (left) and HT-29 cells (right) by immunocytochemistry. CD13 was detected by anti-CD13-FITC antibody (green). The nuclei were stained with Hoechst 33342 (blue). The scale bars represent 20 μm.

The *in vitro* cytostatic effect and cellular uptake were higher in case of Nle-containing conjugate on both cell lines. However, the Lys-containing conjugate showed higher selectivity on tumor cells. None of the conjugates showed either acute or chronic toxicity on mice up to the dose of 25 mg Dau content in conjugates. Dau=Aoa-GFLGK(c[KNGRE]-GG)-NH$_2$ showed higher tumor growth inhibition on CD13+ KS tumor bearing mice, while Dau=Aoa-GFLGK(c[NleNGRE]-GG)-NH$_2$ had higher activity on CD13- but integrin positive HT-29 tumor bearing mice. In the latter case, orthotopically developed tumor model was applied. Based on these results, we can conclude that both NGR-Dau conjugates, as well as free Dau inhibited tumor growth and metastasis development. However, Dau=Aoa-GFLGK(c[NleNGRE]-GG)-NH$_2$ showed higher antitumor and antimetastatic effect against colon cancer compared to Dau=Aoa-GFLGK(c[KNGRE]-GG)-NH$_2$, while its impact on the animal body weight and liver weight was the lowest. Both conjugates demonstrate significant effect on inhibition of proliferation in the primary tumor and inhibition of blood vessels formation making them promising candidates for targeting angiogenesis processes in tumor tissues.

6. Application of cyclic NGR peptides in positron emission tomography (PET)

Aminopeptidase N (APN/CD13) plays an important role in neoangiogenic process in malignancies. Our previous studies have already shown that ^{68}Ga-labelled NOTA conjugated NGR peptide (c[KNGRE]-NH$_2$) specifically bind to APN/CD13 expressing tumors [47]. In this recent study the APN/CD13 specificity of newly synthesized ^{68}Ga-labelled NGR derivatives were evaluated and compared *in vivo* by PET/MRI imaging using hepatocellular carcinoma (He/De) and mesoblastic nephroma (Ne/De) tumor models [48]. PET/MRI and *ex vivo* biodistribution studies were performed 11 ± 1 days after subcutaneous injection of tumor cells and 90 min after intravenous injection of ^{68}Ga-NOTA-c(NGR), ^{68}Ga-NODAGA-c(NGR), ^{68}Ga-NODAGA-c(NGR) (MG1) or ^{68}Ga-NODAGA-c(NGR) (MG2) (**Figure 18**.).
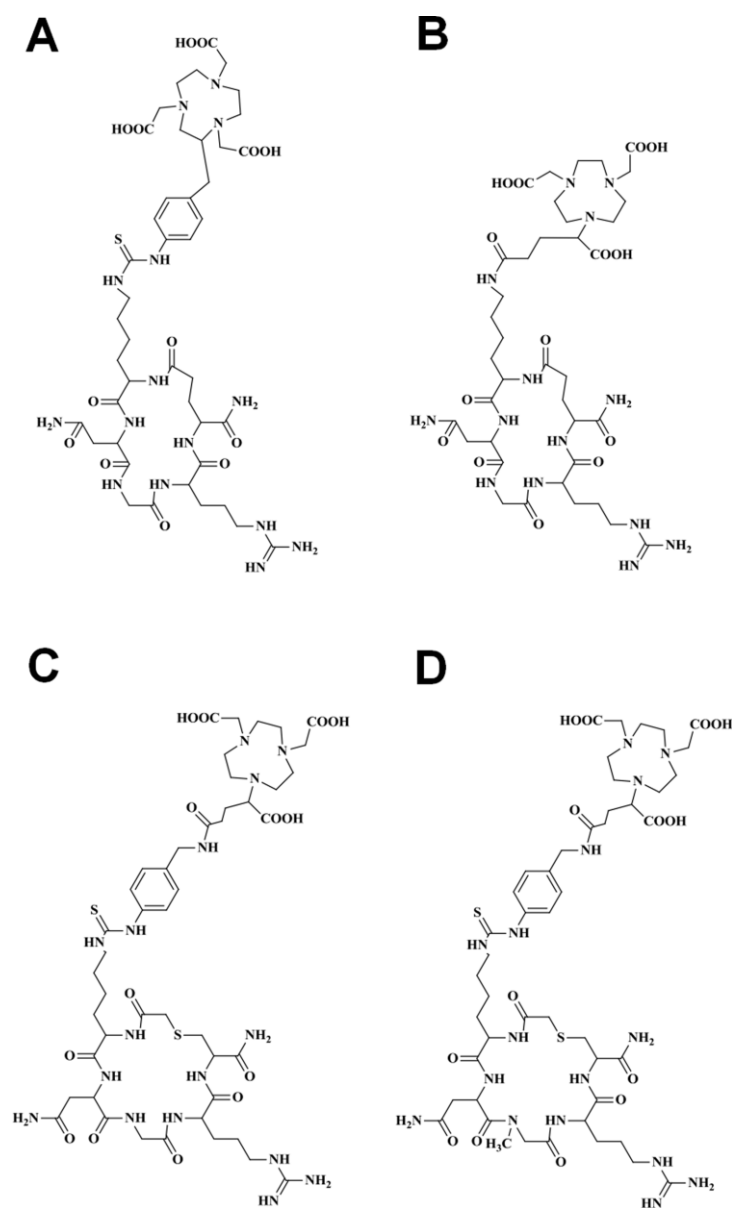
Figure 18. Chemical structures of NOTA-c(NGR) (A), NODAGA-c(NGR) (B), c[CH$_2$-CO-Lys(NODAGA)-Asn-Gly-Arg-Cys]-NH$_2$ (NODAGA-c(NGR) (MG1)) (C), c[CH$_2$-CO-Lys(NODAGA)-Asn-N(Me)Gly-Arg-Cys]-NH$_2$ (NODAGA-c(NGR) (MG2)) (D)

The APN/CD13 selectivity was confirmed by blocking experiments and the APN/CD13 expression was verified by immunohistochemistry. ^{68}Ga-labelled c(NGR) derivatives were produced with high specific activity and radiochemical purity. In control animals, low radiotracer accumulation was found in abdominal and thoracic organs. Using tumor-bearing animals we found that the ^{68}Ga-NOTA-c(NGR), ^{68}Ga-NODAGA-c(NGR), and ^{68}Ga-NODAGA-c(NGR) (MG1) derivatives showed higher uptake in He/De and Ne/De tumors, than that of the accumulation of ^{68}Ga-NODAGA-c(NGR) (MG2) suggesting that Gly cannot be replaced by *N*-Me-Gly derivative (**Figure 19**.). APN/CD13 is a very promising target in PET imaging, however, the selection of the appropriate ^{68}Ga-labelled NGR-based radiopharmaceutical is critical for the precise detection of tumor neo-angiogenesis and for monitoring the efficacy of anticancer therapy.
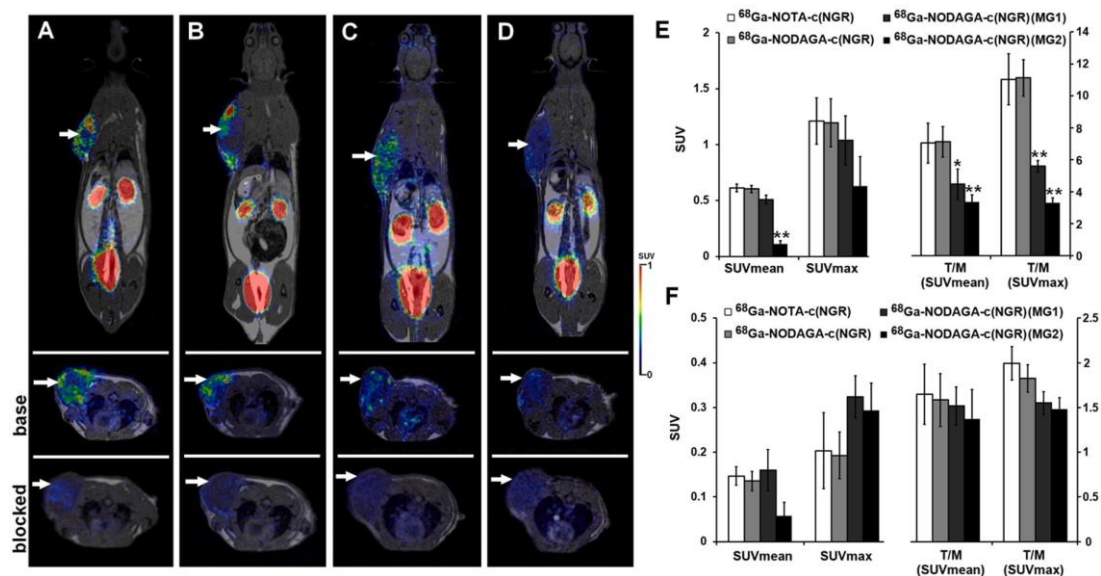
Figure 19. *In vivo* assessment of ^{68}Ga-labelled NGR derivatives uptake of He/De tumors. Representative coronal (upper row) and transaxial (middle row: base; lower row: blocked with unlabeled peptide) PET/MRI images of tumor-bearing rats 90 min after intravenous injection of ^{68}Ga-NOTA-c(NGR) (A), ^{68}Ga-NODAGA-c(NGR) (B), ^{68}Ga-NODAGA-c(NGR) (MG1) (C), and ^{68}Ga-NODAGA-c(NGR) (MG2) (D). Quantitative SUV analysis of base (E) and blocked (F) radiotracer uptake data in Ne/De tumors 90 min post inj. and 11 ± 1 days after subcutaneous injection of He/De tumor cells. Significance level: $p \leq 0.05$ (*) and $p \leq 0.01$ (**). SUV: standardized uptake value; T/M: tumor-to-muscle ratio. SUV values are presented as mean $\pm$ SD. Similar effects were observed on Ne/De tumors as well.

The prepared radio conjugates were used for additional studies. For example, ^{68}Ga-NODAGA-c(NGR) accumulation was observed in both bestatin- and actinonin-treated B16-F10 melanoma tumors compared to the untreated-control tumors. Bestatin inhibited tumor growth and ^{68}Ga-NODAGA-c(NGR) uptake in both tumor models (**Figure 20**.). We could conclude that ^{68}Ga-NODAGA-c(NGR) is

an applicable radiotracer for the *in vivo* monitoring of the efficacy of the APN/CD13 inhibition-based anticancer therapies [49].
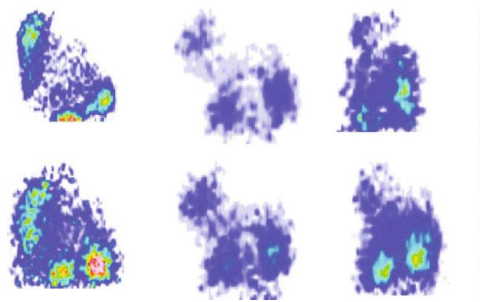
Figure 20. *In vivo* assessment of ^{68}Ga-NODAGA-c(NGR) uptake of control-untreated and actinonin- and bestatin-treated B16-F10 tumors. Representative coronal decay-corrected PET images of control-untreated, bestatin-treated, and actinonin-treated B16-F10 tumor-bearingC57BL/6J mice 5 (upper row) and 10 days (lower row) after tumor cell inoculation and 90 min after intravenous injection of 68Ga-NODAGA-c(NGR).

The higher localization of the ^{68}Ga-NOTA-cNGR radiotracers over ^{68}Ga-NODAGA-RGD in Ne/De tumors was observed in mice (**Figure 21**.). This might suggest that the NGR derivative is better for detection of tumors by recognition of neoangiogenic blood vessels.
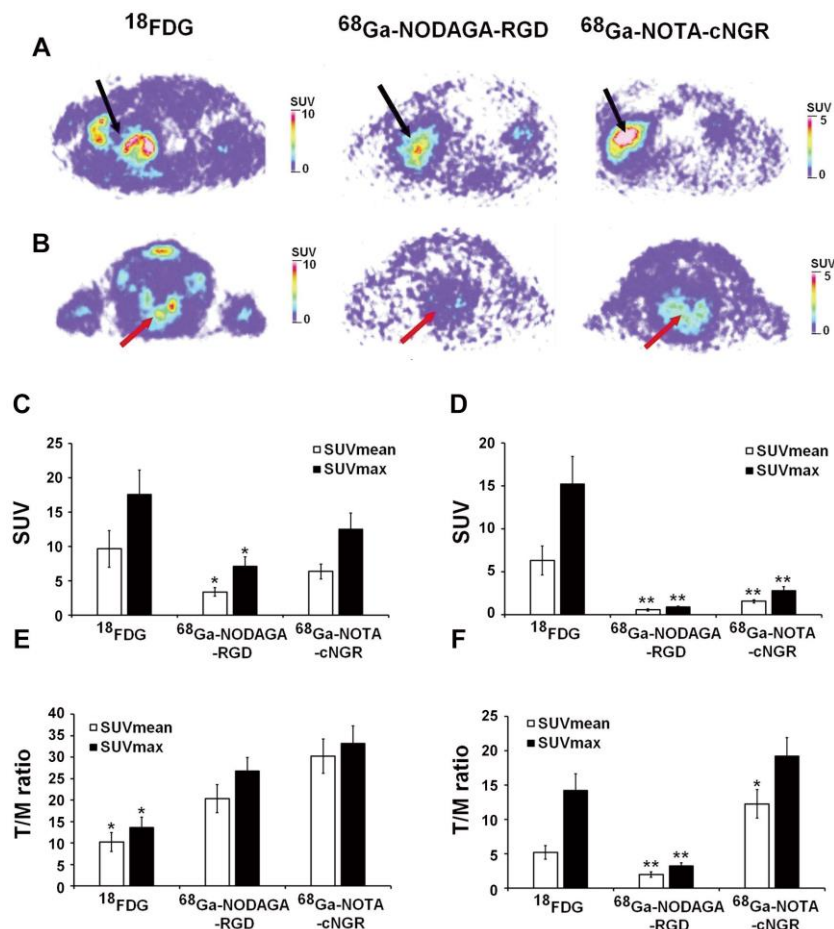

Figure 21. *In vivo* PET imaging studies of Ne/De tumor-bearing rats 8±1 days after the SRCA implantation of metastatic parathymic lymph node from the second experiment. Representative decay corrected transaxial PET images of primary Ne/De tumors located under the renal capsule (A) and metastatic parathymic lymph nodes in

the thorax (B) 50 min after the intravenous injection of [^{18}F]FDG and 90 min after intravenous injection of ^{68}Ga-labelled radiotracers. Quantitative SUV analysis of radiotracer accumulation in the subrenal Ne/De tumors (C and E) and metastatic parathymic lymph nodes (D and F). Black arrows: primary Ne/De tumor, red arrows: parathymic lymph nodes. SUV: standardized uptake value. T/M: tumor-to-muscle ratio. Significance levels: p≤0.05 (*) and p≤0.01 (**). Data is presented as mean±SD; n=3 rats/radiotracer.

By the aid of our radiotracer NGR and RGD conjugates, the ischemia/reperfusion-mediated Aminopeptidase N expression and hypoxia induced integrin expression were detected efficiently [50,51]. Furthermore, the selectivity and activity of additional APN/CD13 specific peptides were compared. From the newly developed radioligands [^{68}Ga]-NODAGA-APRPG-COOH showed comparable parameters on the B16F10 tumor-model than the reference compound [^{68}Ga]Ga-NOTA-c(NGR), and can be a promising candidate for further development. Interestingly, the amidated version was completely inactive [^{68}Ga]-NODAGA-APRPG-CONH$_2$ [52].

7. Sequence modification of homing peptide selected by phage display for HT-29 colon cancer cells to improve the anti-tumor activity of drug delivery systems

In our previous OTKA project, the sequence modification of a heptapeptide VHLGYAT selected by phage display technique was investigated. First Ala-scan was applied to find out the positions where amino acid substitutions are allowed. It was indicated that Gly in position 4 can be changed by Ala. This modification resulted in a conjugate Dau=Aoa-LRRY-VHL**A**YAT-NH$_2$ that had higher antitumor activity that could be explained by the improved cellular uptake property. In the next step that partially was the topic of this new project, positional scanning was made in positions 4 and 6. The Ala amino acids were changed by other amino acids with different characters. The results indicated that the incorporation of apolar amino acids with bulky side chain in these positions increase the cellular uptake (**Figure 22**.) of these conjugates that enhance their antitumor activity [53].
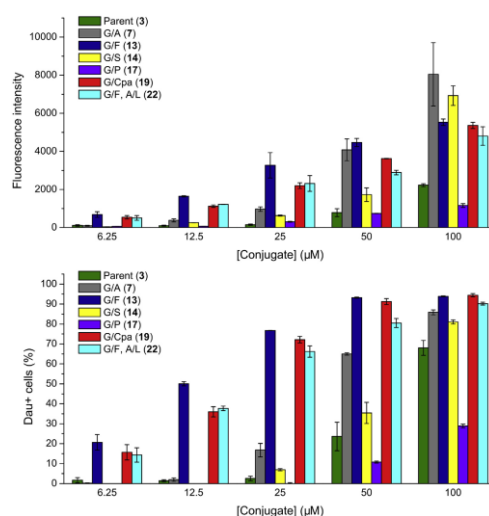
Figure 22. Comparison of the cellular uptake of drug conjugates G/F (13), G/S (14), G/P (17) and G/Cpa (19) and G/F, A/L (22) with parent conjugate (3) and G/A (7) using flow cytometry on HT-29 colon cancer cells. Experiments were performed in duplicates (error bars represent standard deviation).

The most efficient conjugates were Dau=Aoa-LRRY-VHL**F**YAT-NH$_2$, Dau=Aoa-LRRY-VHL**L**YAT-NH$_2$, Dau=Aoa-LRRY-VHL**Cpa**YAT-NH$_2$, and Dau=Aoa-LRRY-VHL**FYL**T-NH$_2$. The IC$_{50}$ values were below 10 μM for these conjugates.

Next to the HT-29 colon cancer cell line the conjugate containing the parent sequence (Dau=Aoa-LRRY-VHLGYAT-NH$_2$ (**3**)) and Dau=Aoa-LRRY-VHL**F**YAT-NH$_2$, (**13**) were investigated on further tumor types. The results showed that the sequence modified conjugate had higher cytostatic effect on all types of cancer (especially on colon, lung, hepatocellular, prostate cancers and melanoma cells) and showed higher selectivity to cancer cells (see MRC-5 data) (**Table 8**.).

Table 8. Specificity study of the cytostatic effect of drug conjugates 3 and G/F (13) compared to free Dau on various cell lines.

Tumor types (cell lines)	Dau (IC$_{50}$; μM)	**3** (IC$_{50}$; μM)	**3** / Dau	**13** (IC$_{50}$; μM)	**13** / Dau	**3** / **13**
Melanoma (mouse B16)	0.0089 ± 0.0053	15.2 ± 3.0	1711.3	**3.0 ± 0.5**	335.4	**5.07**
Prostate (DU145)	0.0245 ± 0.0053	**6.1 ± 2.2**	249.7	**3.5 ± 0.5**	**142.3**	1.74
Lung (H6509)	0.0475 ± 0.0016	**4.4 ± 1.2**	**92.6**	**2.9 ± 0.6**	**60.1**	1.52
Lung (H1975)	0.0133 ± 0.0047	19.3 ± 0.1	1458.7	**3.7 ± 0.8**	279.9	**5.22**
Melanoma (A2058)	0.0332 ± 0.0004	**10.5 ± 5.8**	316.8	**3.5 ± 1.3**	**104.5**	**3.00**
Head and neck(PE/CA PJ41)	0.0258 ± 0.0054	**9.4 ± 3.5**	363.9	**4.3 ± 0.1**	165.7	**2.19**
Head and necki (PE/CA PJ15)	0.0264 ± 0.0050	20.2 ± 4.6	759.3	**7.4 ± 3.4**	277.3	**2.73**
hepatoma (HepG2)	0.0213 ± 0.0009	22.4± 4.4	1052.6	**4.7 ± 0.5**	220.2	**4.77**
Melanoma (M24)	0.0936 ± 0.0258	**15.4 ± 3.7**	164.3	**5.8 ± 0.9**	**61.7**	**2.66**
Breast (MDA-MB-231)	0.0529 ± 0.0103	**6.3 ± 2.5**	**118.8**	**4.6 ± 0.8**	**86.6**	1.37
Melanoma (WM983b)	0.0442 ± 0.0192	**7.1 ± 2.5**	159.8	**5.1 ± 0.4**	**114.6**	1.39
Glioma (U87MG)	0.0279 ± 0.0035	**14.2 ± 3.5**	510.3	**6.6 ± 0.2**	236.9	**2.15**
Lung (A549)	0.0681 ± 0.0227	25.9 ± 2.3	380.1	**5.9 ± 1.5**	**86.1**	**4.39**
Colon (HT116)	0.1271 ± 0.0219	33.6 ± 4.4	264.1	**7.2 ± 0.3**	**57.0**	**4.67**
Prostate (PC-3))	0.0260 ± 0.0071	20.5 ± 0.3	787.5	**5.9 ± 1.6**	226.7	**3.48**
Colon (mouse C26)	0.1260 ± 0.0468	**15.8 ± 2.5**	**125.7**	**8.3 ± 1.0**	**66.0**	1.90
Colon (HT-29)	0.2029 ± 0.0010	30.1 ± 0.3	**148.3**	**11.6 ± 0.1**	**57.1**	**2.60**
Colon(WIDR)	0.2401 ± 0.0363	34.1 ± 3.2	**141.8**	**15.1 ± 2.9**	**62.8**	**2.26**
Ovarian (OVCAR-3)	0.4729 ± 0.0636	**13.8 ± 0.5**	**29.3**	**11.3 ± 2.6**	**24.0**	1.22
Breast (MCF-7)	0.2860 ± 0.0247	22.2 ± 9.2	**77.6**	**11.1 ± 3.8**	**38.8**	**2.00**
Breast (mouse 4T1)	0.0408 ± 0.0068	34.2 ± 0.4	837.4	**11.6 ± 3.6**	284.6	**2.95**
Colon (HT-25)	0.1564 ± 0.0721	33.2 ± 3.5	212.4	**15.4 ± 2.8**	**98.5**	**2.16**
Pancreatic (PANC-1)	0.4667 ± 0.0366	31.7 ± 4.5	**68.0**	26.9 ± 8.1	**57.7**	**1.18**
Fibroblast (MRC-5)	0.2547 ± 0.0006	**39.3 ± 24.6**	**154.2**	**52.1 ± 1.7**	**204.6**	**0.75**

The *in vivo* experiments confirmed these observations. The tumor growth inhibition of conjugate **13** was significantly higher on orthotopically developed HT-29 colon tumor than it was observed in case of conjugate **3** with the parent homing peptide. Conjugate **13** showed higher antitumor activity and lower toxicity than the free drug (**Figure 23.**).
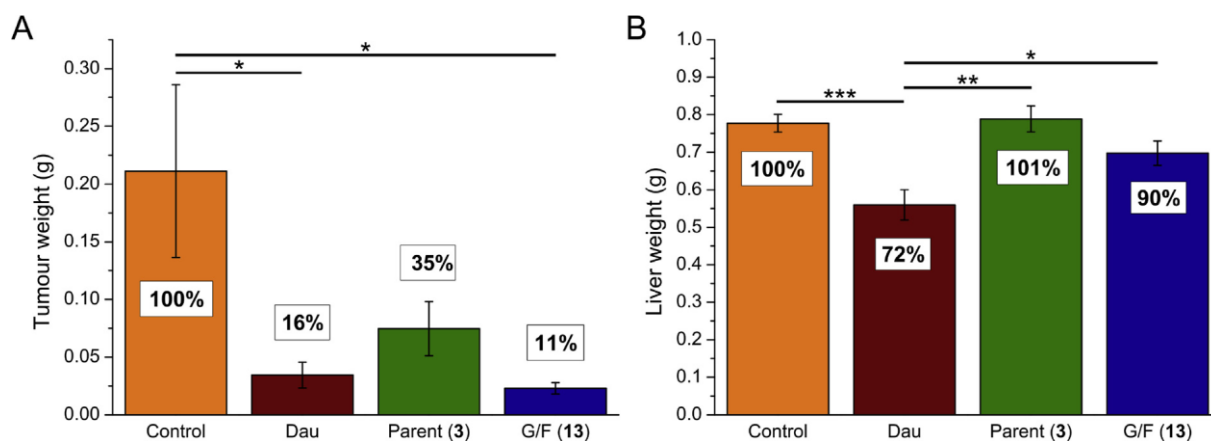
Figure 23. Comparison of tumor (A) and liver (B) weights during in vivo tumor growth inhibition experiment. 8-8 mice per group were treated with solvent, free Dau, drug conjugates3 or 13 from day 13 after tumor transplantation (established by HT-29 colon cancer cells). Tumors and livers were weighed after termination of the treatments. Note that daunomycin group was terminated on day 23 after tumor transplantation due to significant weight loss of the animals. Bars represent average of weights ± standard error of mean (note that because of the death of some animals before termination, N ¼ 7, 7, 6 and 8 from left to right). Statistical analysis was performed by Mann-Whitney test. *, ** and *** mean significant at $p < 0.05$, $p < 0.01$ and $p < 0.001$, respectively.

During the selection of the VHLGYAT heptapeptide by phage display, Zhang et al. did not identify the receptor on HT-29 cancer cells [54]. The selectivity of the peptide was not checked on a broad spectrum of tumour types either. Interestingly, our measurements on different types of cancer cell lines did not show selectivity to HT-29 cells. Therefore, we searched sequence homology in the literature. In the manuscript published by Fourie et al., we found two peptides A6R (ASHLGLAR) and HbS (VHLTPVEK) that have overlapping sequence with our parent peptide (see in bold) [55]. Both of them bind to Hsp70 but the de novo A6R peptide has higher affinity. HbS peptide is originated from the N-terminus of hemoglobin B chain [56] and it was also indicated that hemoglobin interacts with cytosolic Hsp70 efficiently [57]. In our experiments, the replacement of Gly to Thr and Ala to Leu increases the biological effect, furthermore, these changes also enhance the similarity of the sequence with Hbs peptide. According to the literature, heat shock protein 70 (Hsp70) is overexpressed in a large variety of different tumor types and it is localized not only intracellularly, but also tumor selective Hsp70 expression in the plasma membrane was determined [58]. A membrane Hsp70 positive tumor phenotype is associated with aggressiveness and therapy resistance of cancer and the membrane bound Hsp70 plays a pivotal role in eliciting anti-tumor immune response. Furthermore, it can be a good target for targeted tumor therapy. All of these make a strong suggestion that VHLGYAT based homing peptides might be recognized by membrane bound Hsp70, that was partly confirmed by proteomic studies.

8. Development of highly active HER-2 receptor recognizing peptide

Human epidermal growth factor (HER2) is a transmembrane tyrosine kinase receptor that is frequently overexpressed in breast cancer. Its increased level prognoses a poor patient outcome and a high mortality

rate. Despite the widening spectrum of therapies that are becoming available to treat HER2+ breast cancer, its side effects and resistance still make this protein a valuable object of research in targeted tumor therapy [59]. The role of tumor-targeting peptides has become more and more prominent in the last few decades due to their simple synthesis and pharmacokinetic properties. Karasseva et al. identified a hexapeptide (KCCYSL) that most frequently occurred in an affinity-selected phage population against the extracellular domain of HER2. This peptide demonstrated a high affinity and specificity for HER2 and also bound to HER2-expressing cells [60]. Hence, we selected this peptide as one of the starting points of our study to create new, modified peptides to enhance HER2 binding affinity. Another regularly used method to pick peptides that bind specifically to a target is molecular dynamics (MD) simulation. Geng et al. used this method to identify peptides at the extracellular domain of HER2 that are involved in dimerization. These peptides were then used to construct a "One bead one compound" (OBOC) library. After screening and sequencing, peptide affinity and specificity were analyzed. This resulted in the obtainment of 72 highly similar 17-mer peptides with a high binding affinity to the HER2 receptor [61]. The central part of these peptides was rather conservative, while the terminals showed a bit more variability. Among them, CDTFPYLGWWNPNEYRY and CKTIYYLGYYNPNEYRY showed the highest affinity to HER2. As the N-terminal part of the peptides (especially the latter one) showed sequence similarities with the KCCYSL peptide, we decided to synthesize combined peptides where the modified KCCYSL sequence precedes GYYNPN. We then compared their binding to the extracellular domain of HER2-expressing cells. Our aim was to optimize the peptide structure in a way that created specific, high affinity HER2 binding peptides that could be used in either diagnostics or in drug delivery and tumor-targeting in the future.

The results indicated that the cysteines in the sequence of KCCYSL can be replaced by serines without significant influence of cellular uptake. In addition, the combined CF-KSCYSLGYYNPT-NH$_2$ (cP(SC)_P(YY)) peptide showed significantly higher uptake by HER2+ breast cancer cells (MDA-MB-453) in comparison with any of the monomers (**Figure 24**.). Furthermore, the substitution of cysteines by alanines resulted in a compound (CF-KAAYSLGYYNPT-NH$_2$ (cP(AA)_P(YY)) with extremely high binding affinity and cellular uptake (membrane localization). This could be explained by the higher α-helix formation propensity of the later peptide to the others (**Figure 25**.). It was also demonstrated that the order of the sequences cannot be changed (CF-GYYNPTKAAYSL-NH$_2$ (cP(YY)_P(AA)), because the binding activity was completely decreased similarly to scrambled peptide derivative.

In accordance with our observations, the further aim of our study is to possibly apply the selected combined homing peptides for tumor diagnostics (*e.g.,* positron-emission tomography) or the selective delivery of radiotracers with therapeutic activity. In addition, the application of extracellular enzyme (elastase, matrix metalloproteinases) cleavable spacers between the homing peptide and an antitumor agent might be a good choice for the development of conjugates as drug delivery systems.
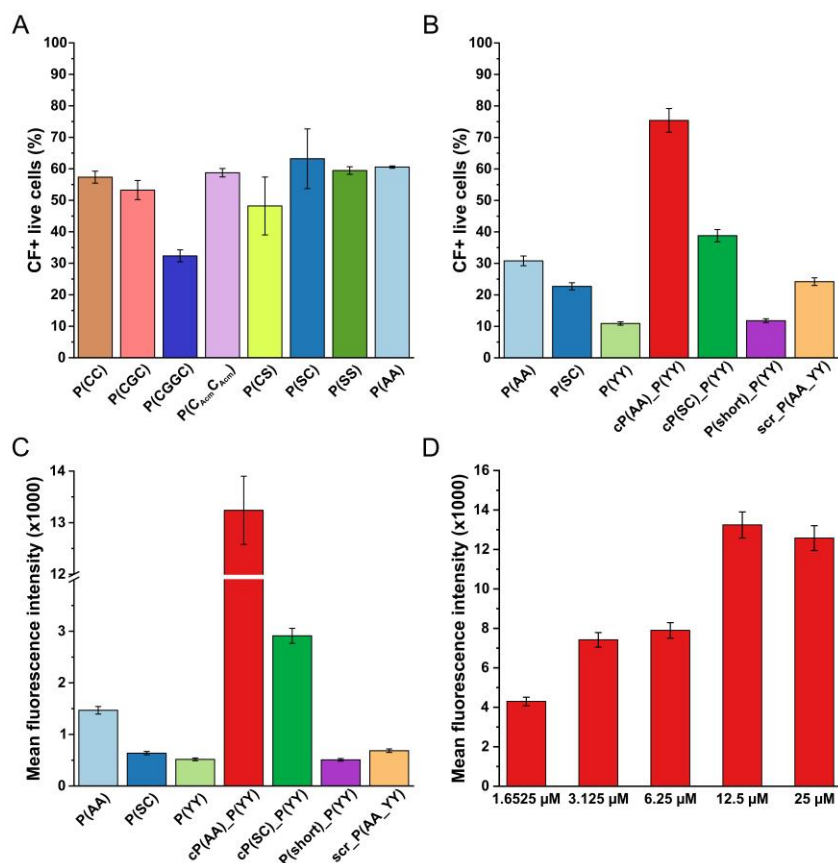
Figure 24. Cellular uptake study of CF-labeled HER2 binding peptides using MDA-MB-453 breast cancer cells. (A) Comparison of the first set of peptides using 1 h incubation time and a concentration of 100 µM. (B, C) Cellular uptake (percentage of CF+ live cells and mean fluorescence intensity) of the most promising conjugates from the first set of peptide, the peptide chosen from the MD simulation and OBOC library and combined peptides using 3 h incubation time and a concentration of 12.5 µM. (D) Concentration dependence of cellular uptake of conjugate cP(AA)_(YY), mean fluorescence intensity after 3 h incubation. Flow cytometry was measured by a BD LSR II flow cytometer, mean and standard deviation of two parallels are depicted, the experiments were repeated twice.
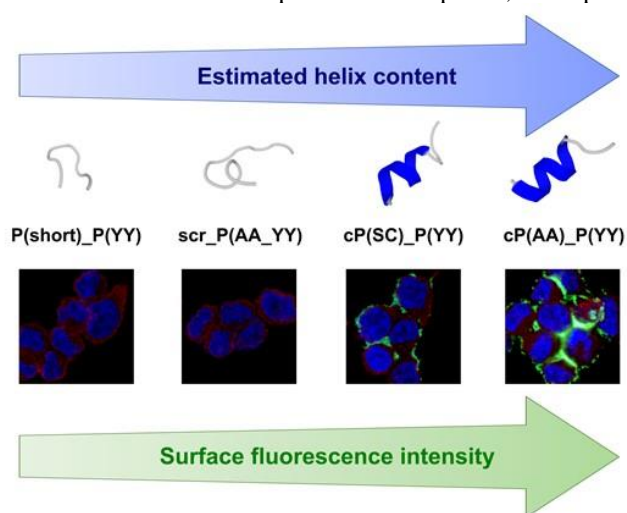
Figure 25. Estimated α-helical content of HER2-binding peptides is proportional to the fluorescence intensity detected on the surface of MDA-MB-453 cells incubated with CF-labeled peptides. Secondary structure estimation of the peptides was performed by PEP-FOLD3 de novo secondary structure prediction server. The color grey shows disordered regions, predicted α-helical content is marked with blue. Cell imaging was carried out by confocal microscopy where CF signal and nucleus staining can be seen by green and blue, respectively. HER2 was detected with anti-HER2 antibody and TRITC-conjugated secondary antibody (red).

8. Phage display-based homing peptide - daunomycin conjugates for selective drug targeting to Pancreatic Ductal Adenocarcinoma (PDAC)

The Pancreatic Ductal Adenocarcinoma (PDAC) is one of the most aggressive and dangerous cancerous diseases, leading to a high rate of mortality. Therefore, the development of new, more efficient treatment approaches is necessary to cure this illness. Peptide-based drug targeting provides a new tool for this purpose. Previously, a hexapeptide Cys-Lys-Ala-Ala-Lys-Asn (CKAAKN) was applied efficiently as the homing device for drug-loaded nanostructures in PDAC cells [63]. In this research, Cys was replaced by Ser in the sequence and this new SKAAKN targeting moiety was used in conjugates containing daunomycin (Dau) [64]. Five different structures were developed and tested. The results indicated that linear versions with one Dau were not effective on Panc-1 cells in vitro; however, branched conjugates with two Dau molecules showed significant antitumor activity (**Table 9**. and **Figure 26**.).

Table 9. Characterization of the cytotoxicity of the conjugates on the PANC-1 cell line

Code	Compounds	Viability[a] (%) at 10^{-5} M concentration, after 72 h incubation
1	*Dau=Aoa*-SKAAKN-*OH*	112.5 ± 5.1
2	*Dau=Aoa*-KSKAAKN-*OH*	154.2 ± 7.1
3	*Dau=Aoa*-GFLG-KSKAAKN-*OH*	105.1 ± 1.9
4	*Dau=Aoa*-GFLG-K(*Dau=Aoa*)SKAAKN-*OH*	0.1 ± 0.1
5	*Dau=Aoa*-GFLG-K(*Dau=Aoa*-GFLG)SKAAKN-*OH*	31.3 ± 1.8

[a] Cell index (CI) values of the treated cells are normalized to the CI values of the control wells and expressed as percentages. Data are given as mean values ± standard deviation (SD), (n=3).
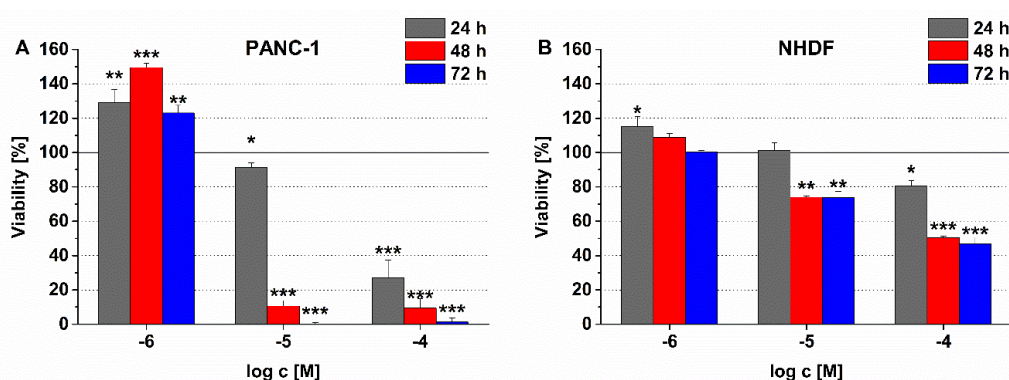
Figure 26. Comparison of the time and concentration dependent effect of conjugate 4 on (A) PANC-1 and (B) NHDF (normal human dermal fibroblast) cell viability. Data shown are mean of 3 parallels ± SD. The significance levels are the following: *: $p < 0.05$, **: $p < 0.01$, ***: $p < 0.005$.

Differences in the antitumor effect of the conjugates could be explained with the different cellular uptake and lysosomal degradation (**Figure 27**. and **Figure 28**.). The most efficient conjugate was Dau=Aoa-

GFLG-K(Dau=Aoa)SKAAKN-OH (conjugate **4**) that showed high binding efficacy and cellular uptake as well as efficient release of appropriate Dau containing metabolites in lysosomal homogenate.
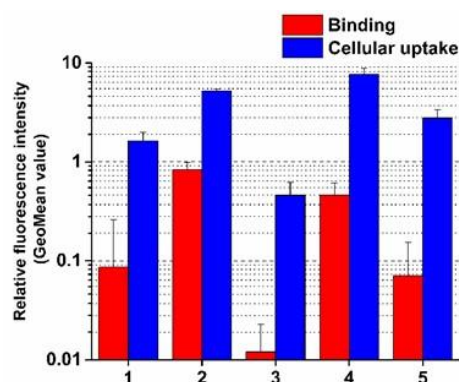
Figure 27. Binding affinity and cellular uptake of conjugates on PANC-1 cells. Binding and cellular uptake of the compounds were studied at 10^{-5} M concentration. GeoMean Data shown are mean of 2 parallels ± SD.
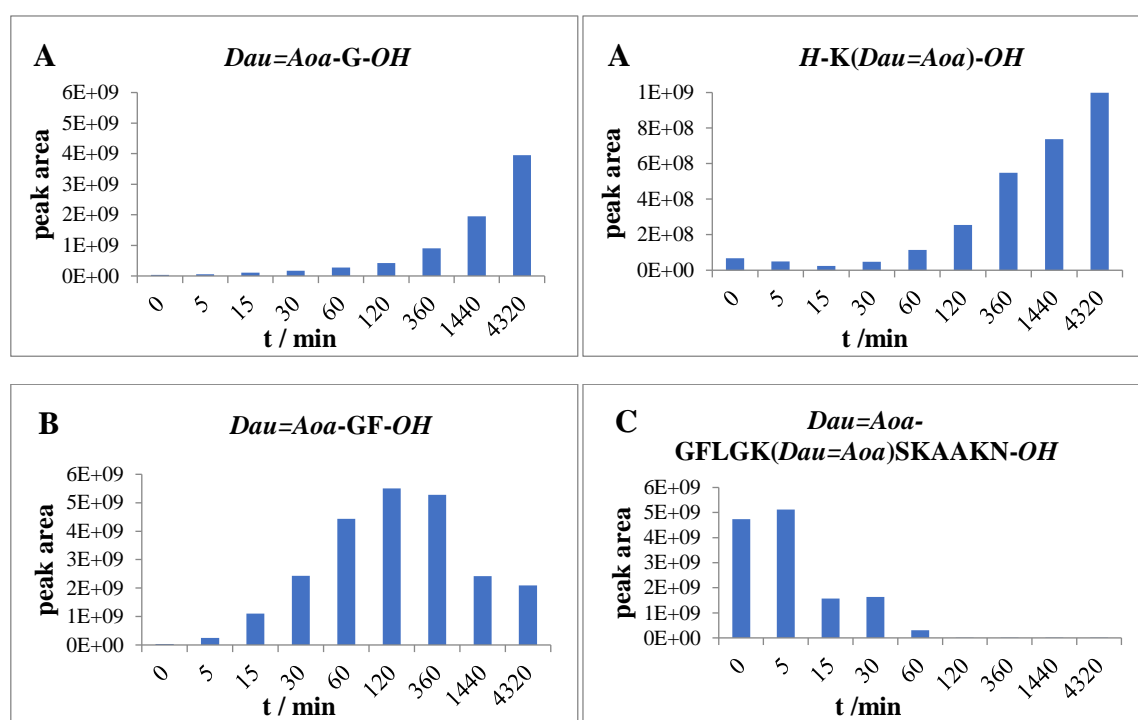
Figure 28. Time-dependent LC-MS intensity change of various molecules during the enzymatic degradation study of conjugate 4: (A) Release of the smallest Dau-containing metabolite; (B) Intensity of the Dau=Aoa-GF-OH metabolite; (C) Time-dependent decrease in the amount of the intact conjugate **4**.

Our results indicate that at the development of peptide-drug conjugates, not only the cellular uptake of the conjugates but also the effective release of the active metabolite should be taken into account. Release of active metabolites was shown to depend highly on the structure of the conjugate.

The most efficient conjugate was Dau=Aoa-GFLGK(Dau=Aoa)SKAAKN-OH (conjugate **4**) in *in vitro* experiments, and it was selected for further *in vivo* studies. In contrast to the free drug, the conjugate **4**

did not show any toxicity during the treatment but elicited significant >30% tumor growth inhibition on PANC-1 bearing mice (**Figure 30.**).

The results suggested that SKAAKN peptide-based drug delivery systems could be promising constructs alone or in combination for the treatment of pancreatic cancers.
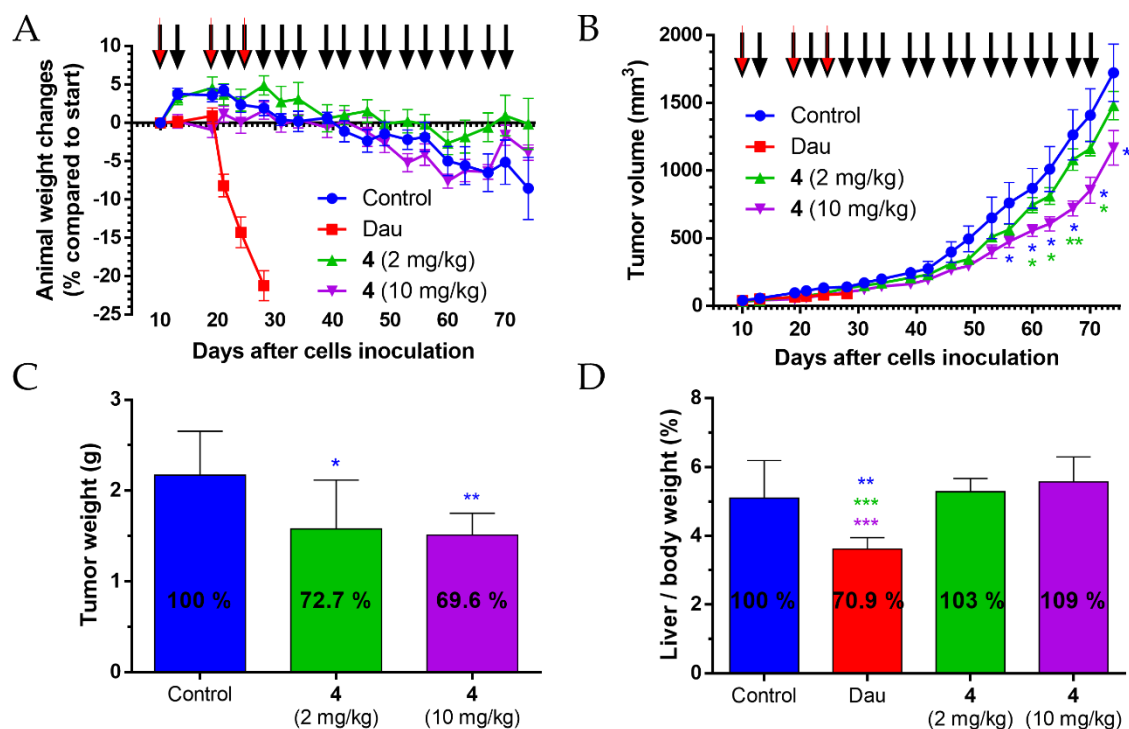

Figure 30. Effect of conjugate **4** (2 mg/kg and 10 mg/kg Dau-content, 18 treatments, black arrows) and free Dau (1 mg/kg, 3 treatments, red arrows) in subcutaneous PANC-1 human pancreatic carcinoma bearing mice. (**A**) Animal body weight changes (percentage compared to the start of the experiment, average ± SEM). (**B**) Tumor volume (mm³, average ± SEM). (**C**) Tumor weight (grams, average ± SD) after termination of the experiment, 74 days subsequent to cell inoculation. (**D**) Liver weight/body weight ratio (percentage, average ± SD) after the termination of the experiment, 74 days after cell inoculation for the control and the conjugate treated groups, while 28 days after cell inoculation for the free Dau-treated group. 7 animals per group. Statistical analysis was performed by the Mann–Whitney test. *, ** and *** mean significant at p ≤0.05, p ≤0.01 and p ≤0.001, respectively. * blue and green mean significant difference of conjugate **4** (10 mg/kg) treated group compared to the control and conjugate **4** (2 mg/kg) groups, respectively (B). * blue mean significant difference of conjugate **4** (2 and 10 mg/kg) treated groups compared to the control (**C**). * blue, green, and purple mean significant difference of free Dau-treated group compared to the control and conjugate **4** (2 and 10 mg/kg) groups, respectively (**D**).

Recently we investigated SREKA homing peptide to increase the selectivity Dau-loaded liposomes [65]. A new method was developed for conjugation of SREKA peptide to DSPE-PEG derivatives used for liposome formation. SREKA was modified by aminooxiacetyl moiety at its N-terminus and in a

chemoselective reaction oxime linkage was formed with aldehyde functionalized DSPE-PEG. Liposomes decorated with different level of SREKA or CREKA (that was described in the literature) wwere compared. We provided evidence that production yield and conjugation abilities of SREKA are better than CREKA's which significantly reduces costs in case of mass production for clinical use. Moreover, we compared the anti-tumorigenic effect of SREKA-targeted liposomes to that of CREKA-targeted ones. Our results exhibit no statistical difference between SREKA- and CREKA-modified liposome formulations, but both of them significantly decrease tumor progression and metastases without considerable toxicity. Their efficacy was significantly higher than it was observed in case of the free Dau and Dau-loaded non-targeted (NP) liposome (**Figure 31**.). The manuscript of this project has been sent for publication.
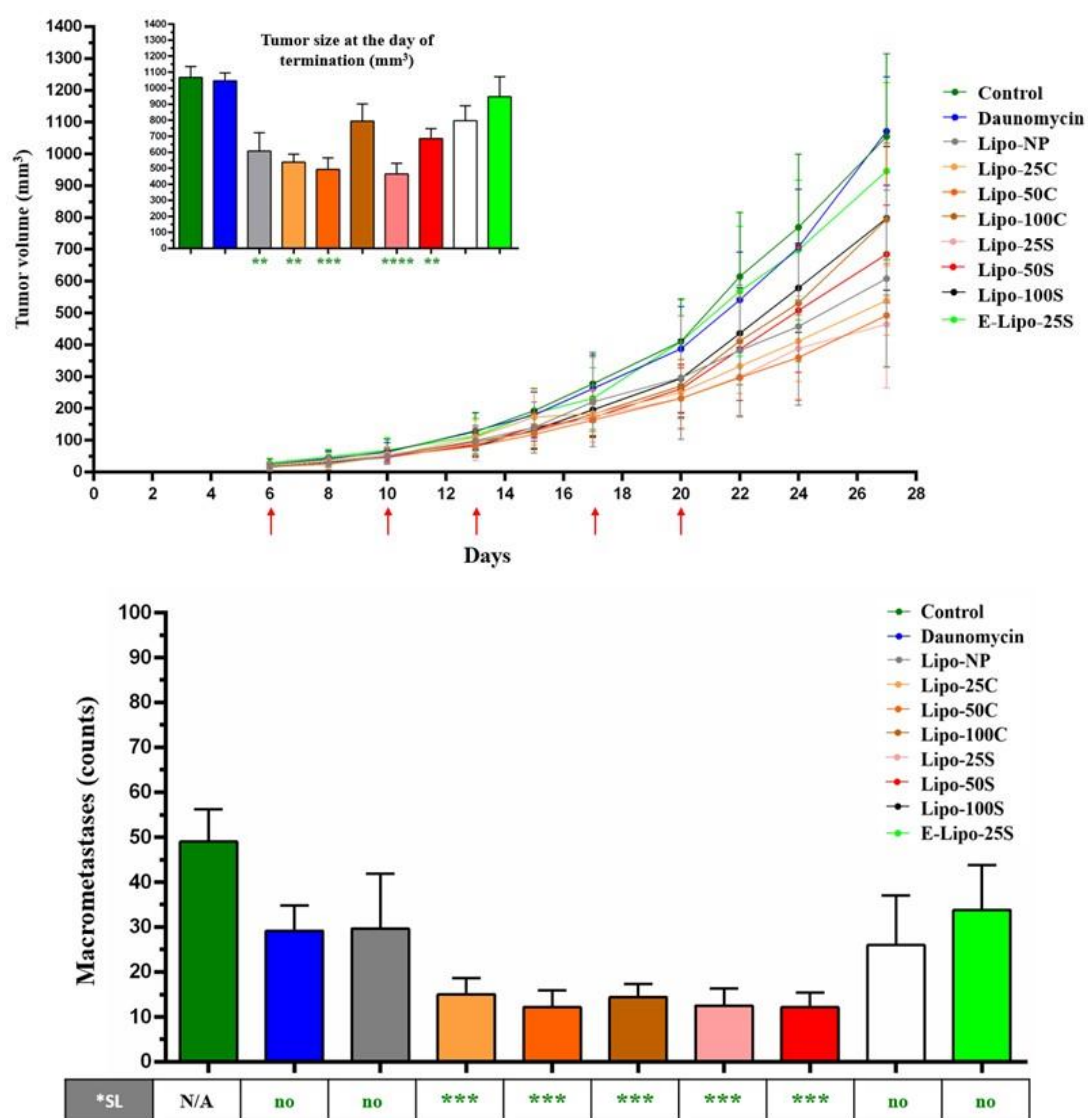
Figure 31: Inhibition of tumor expansion. (A) Change of primary tumor size of mice treated with liposome formulations and free drug. Tumor volume is represented in mm^3. *SL = Significance level. Error bars represent mean ± SEM. (B) Number of metastatic nodules in lung of mice. *SL = Significance level. Error bars represent the mean ± SEM ($n > 5$, ***$p < 0.001$).

9. Influence of the daunomycin position on bioactivity in Angiopep-2 – drug conjugates

The BBB is a semipermeable system and therefore most of the active substances are poorly transported through this barrier resulting in decreased therapeutic effects and causing a major challenge in the treatment of brain tumors. Angiopep-2 (TFFYGGSRGKRNNFKTEEY) is a peptide that was shown to be a ligand of the low-density lipoprotein receptor-related protein-1 (LRP1). It can cross the blood-brain barrier *via* receptor-mediated transcytosis and simultaneously target glioblastoma, thereby dual targeting may be achieved [66]. Angiopep-2 contains three amino groups (two lysine side chains and the *N*-terminus), and all these groups were used in previous studies to produce drug-peptide conjugates [67,68], but the role and importance of each position have not yet been investigated. Hence, we studied the number and position of the drug molecules in Angiopep-2 based conjugates [69,70]. Conjugates containing one, two, and three daunomycin molecules conjugated *via* oxime linkage in all possible variations were prepared. We developed a method for the synthesis of all compounds starting from one batch and using chemoselective protecting scheme (**Scheme 2**.).
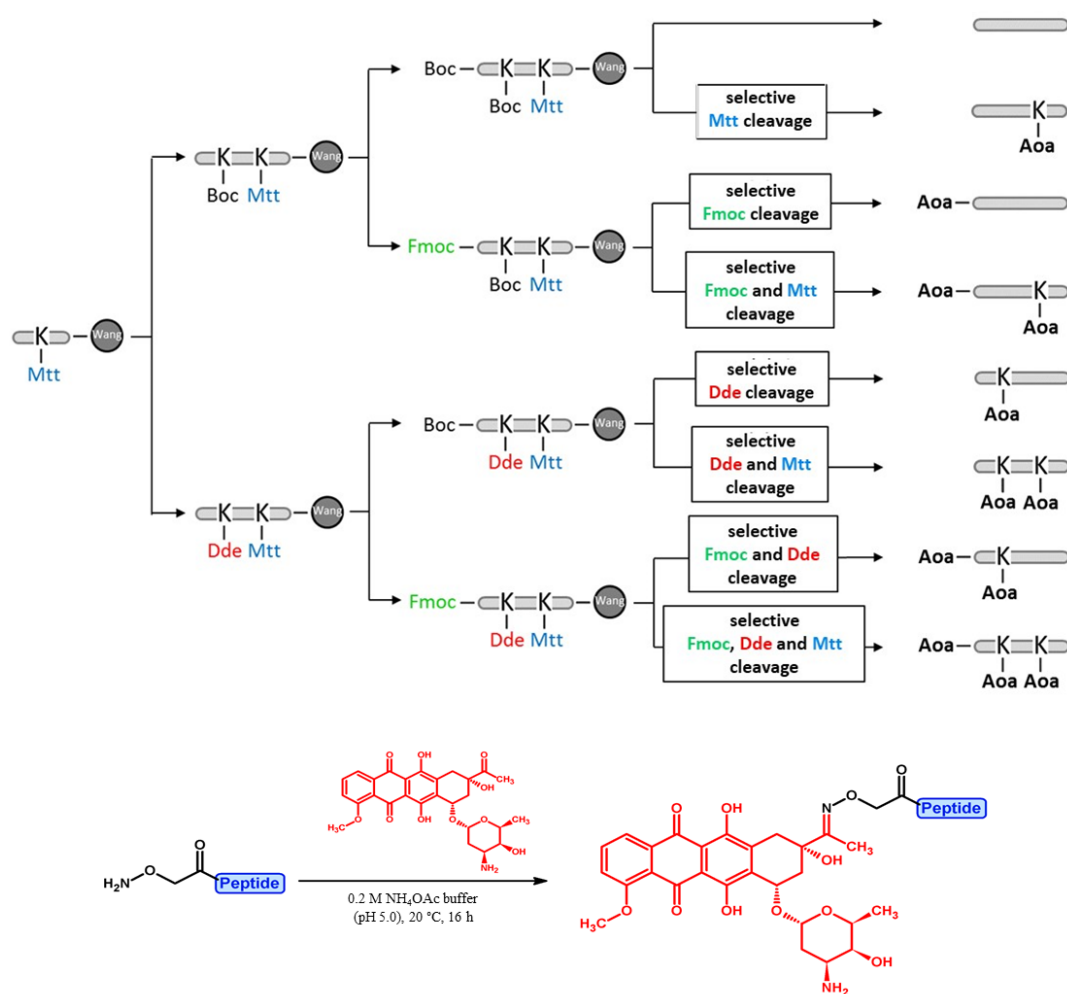

Scheme 2. Synthetic protocol of different Angiopep-2 – daunomycin conjugates using orthogonal side chain protecting groups

The *in vitro* cytostatic effect and cellular uptake of the conjugates with various structures were investigated on U87 human glioblastoma cells (**Table 10**.). Degradation and drug release studies in the presence of rat liver lysosomal homogenate were also performed to better understand the structure-activity relationship. These measurements allowed us to study the cleavage sites of the degradation and the smallest metabolites were also determined. We could demonstrate that the increasing number of the drug molecule does not necessarily increase the efficacy of the conjugates, and we proved that the modification of the different conjugation sites results in different biological effectiveness. The substitution of ^{15}Lys significantly decreased the cellular uptake (**Figure 32**.), while conjugates containing a drug molecule on ^{10}Lys (but not on ^{15}Lys) showed outstanding internalization ability, but the drug release was quite poor. This could be increased by the incorporation of GFLG spacer between the homing peptide and drug molecule. Conjugates with the best antitumor activity had a drug molecule attached to the *N*-terminus.

Table 10. The measured IC_{50} values of the free Angiopep-2 peptide and the Angiopep-2 − daunomycin conjugates

Code	Compound	IC_{50} / μM
1	H-TFFYGGSRGKRNNFKTEEY-OH	> 50
2	H-TFFYGGSRGKRNNFK(Dau=Aoa)TEEY-OH	30.2 ± 6.4
3	Dau=Aoa-TFFYGGSRGKRNNFKTEEY-OH	10.9 ± 2.8
4	H-TFFYGGSRGK(Dau=Aoa)RNNFKTEEY-OH	24.0 ± 5.9
5	Dau=Aoa-TFFYGGSRGKRNNFK(Dau=Aoa)TEEY-OH	32.3 ± 8.1
6	H-TFFYGGSRGK(Dau=Aoa)RNNFK(Dau=Aoa)TEEY-OH	21.6 ± 5.4
7	Dau=Aoa-TFFYGGSRGK(Dau=Aoa)RNNFKTEEY-OH	7.8± 6.3
8	Dau=Aoa-TFFYGGSRGK(Dau=Aoa)RNNFK(Dau=Aoa)TEEY-OH	23.6 ± 6.3
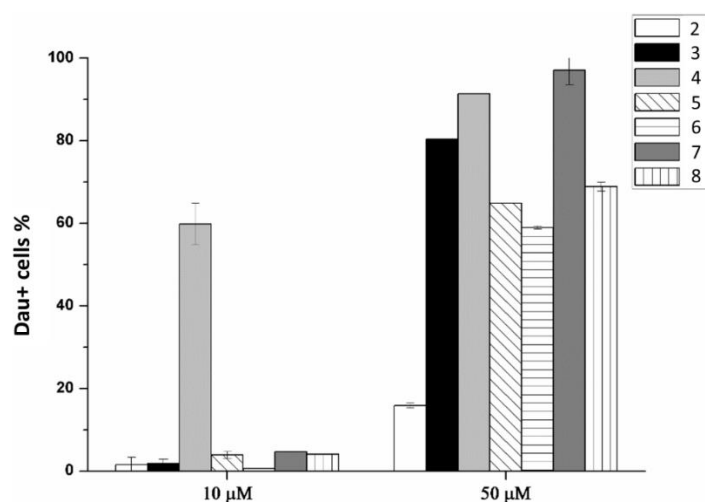
Figure 32. *In vitro* cellular uptake of Angiopep-2 − daunomycin conjugates at 10 and 50 μM

Using this obtained knowledge in the future may help with the design and synthesis of more effective Angiopep-2 – drug conjugates. Manuscript was sent to J. Controlled Release for publication.

10. Optimization of Pep-1 targeting peptide to improve the cellular uptake by glioblastoma cells

Glioblastoma multiforme (GBM) is one of the most aggressive and most frequent primary brain tumors. Its treatment is difficult because of some well-known factors: the brain has a limited ability to repair itself, and any damage may be irreversible, therefore surgery is dangerous, and the complete removal of the tumor is difficult. In addition, gliomas are quite resistant to conventional therapies, and the inadequate penetration of drugs in the blood–brain barrier restricts these treatments as well [71].

GBM tumors can specifically be targeted using Interleukin-13 receptor subunit α2 (IL-13Rα2), a receptor that is overexpressed in the major of patients with GBM but is absent in normal brain tissue [72]. The levels of IL-13Rα2 expression correlates with brain tumor grades and is a prognostic indicator of poor patient survival. Apart from GBM, this receptor is reported to be overexpressed in kidney, head and neck, gastric, ovarian and prostate cancers, adrenocortical carcinoma and Kaposi's sarcoma, as well.

Targeting IL-13Rα2 for cancer therapy has been the focus of numerous studies [73]. Peptides are proper targeting agents and offer several potential advantages: they are small and relatively easy to synthesize, are usually nonimmunogenic, and have attractive pharmacokinetic properties. Peptide sequences targeting IL-13Rα2 have already been identified by studying the binding sites of IL-13 and by phage-display [74]. Pep-1 (CGEMGWVRC) was identified in a disulfide-constrained heptapeptide phages display library and did not match with any IL-13 sequences. It was found that the peptide was internalized in 15 min, furthermore, IL-13 did not compete the Pep-1 binding, indicating that the peptide might have a different binding site than the native ligand. It was also shown that the linear peptide bound to IL-13Rα2 more avidly than the disulfide-constrained form and was also more efficient for *in vitro* and *in vivo* targeting. Pep-1 was used as a targeting ligand for PET imaging, alpha particle therapy, and to develop glioma targeting drug delivery systems through chemical bonding with PEG-PLGA nanoparticles, PEG-PAMAM nanoparticles, self-assembled nanoparticles, and nanoliposomes.

In this study, we investigated systematic modifications in the sequence of Pep-1 by preparing fluorescent conjugates and testing them in in vitro cellular uptake studies. Cysteines at the N-terminal can cause rapid oxidization/dimerization under slightly basic conditions, especially in derivatives with free amino group on the cysteine, while this effect is decreased in the acetylated derivatives [75]. Due to this problem, we systematically studied the relevance of the cysteines by omitting the *N*- and/or the *C*-terminal cysteines from the sequence. Furthermore, we examined the importance of the free *N*-terminal by the presence or absence of acetylation.

The methionine side chain is susceptible to oxidation under acidic conditions with formation of the two diastereomeric sulfoxides, which generally is accompanied by a significant loss of bioactivity. Additionally, this side reaction can cause many synthetic problems as well. The isosteric replacement of methionine by norleucine (Nle) is often used in peptides and proteins, since the structure and the

bioactivity usually do not change significantly [76]. Hence, we examined the effect of the methionine oxidation, the methionine elimination and the change to norleucine in some of the sequences. Furthermore, we were interested in the shortest peptide sequence that has an *in vitro* biological effect, therefore truncated derivatives were also prepared (**Figure 33**.).
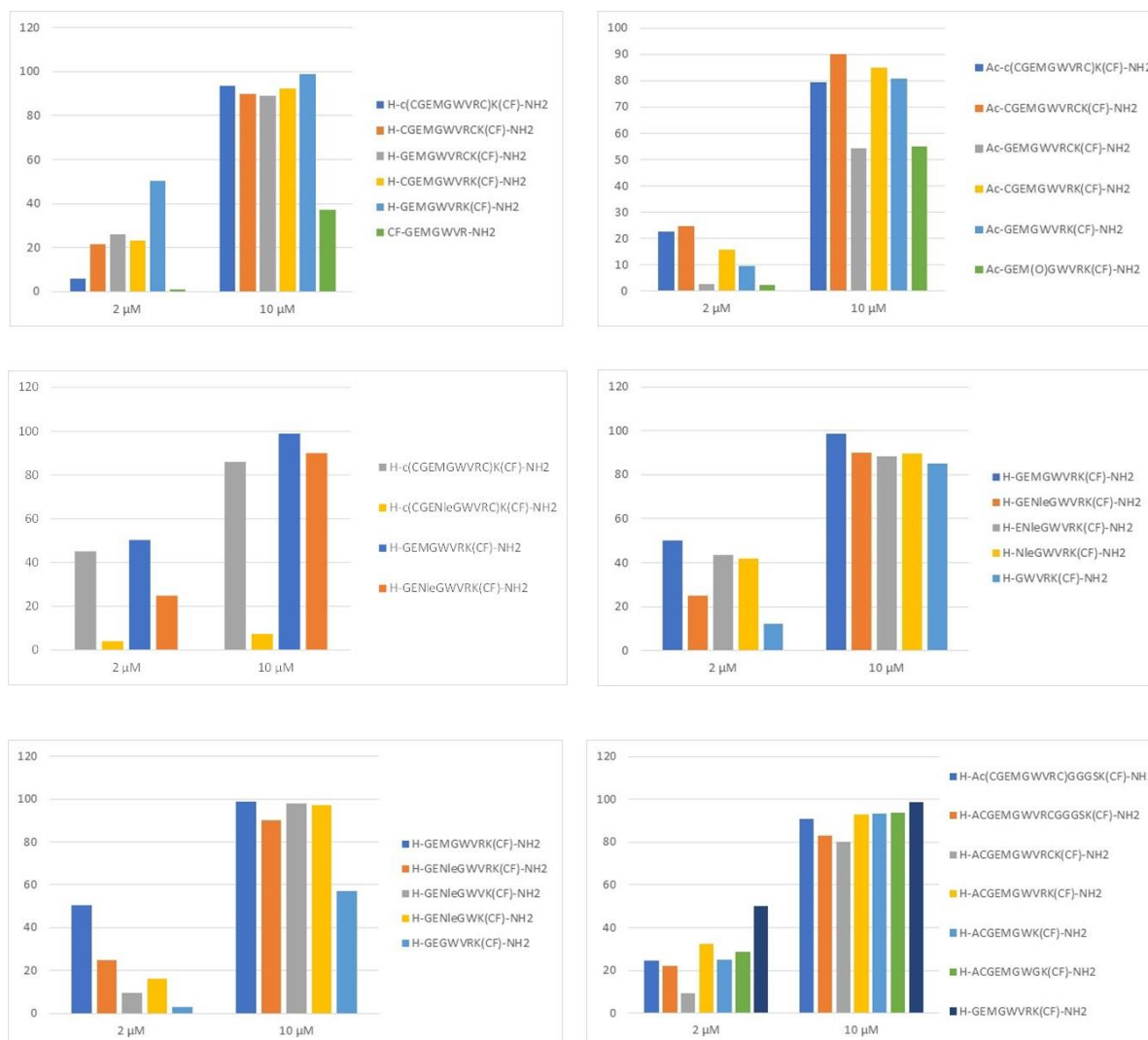
Figure 33. Cellular uptake of carboxyfluorescent labelled Pep-1 derivatives (percentage of CF+ cells are shown)

The results indicated that many of the modified analogs can enter the cells efficiently at low (2 μM) concentration. The replacement of Met by Nle decreased the cellular uptake especially in cyclic version. In addition, the oxidation of Met to sulfoxide had negative influence on the cellular uptake. Interestingly, the removal of cysteines from the termini that resulted linear chain of Pep-1 was taken up by cells more efficiently. It was also demonstrated that the attachment of CF to the *N*-terminus is not allowed, therefore it was coupled to the side chain of an extra Lys incorporated to the *C*-terminal part of the peptide. The acetylation of the *N*-terminal amino group also decreased the cellular uptake. The truncation of Gly-Glu dipeptide from the *N*-terminus is mandatory, but the shortening of the *C*-terminal part led to the decrease

of cellular uptake. Some additional modification suggested by literature data was not suitable to improve the cellular uptake of the Pep-1 analogs.

In conclusion these data provide us a good tool to select effective homing peptides for drug targeting. The development of Dau conjugates is in progress.

11. Effect of uPAR inhibitor peptides for migration and motility of cancer cells

Six uPA (urokinase-type plasminogen activator or urokinase) derived peptides (H1, WX-360, AE-105, UK-202, A6 and [SRSSY]$_{cyclo}$) were synthetised, which may inhibit metastasis, according to literature [77-82]. These peptides have never been compared in the same *in vitro* model system. Therefore, their biological effect was measured on uPA receptor (uPAR) positive A2058 and M1/15 human melanoma cell lines (**Figure 34**.) with different metastatic activity.
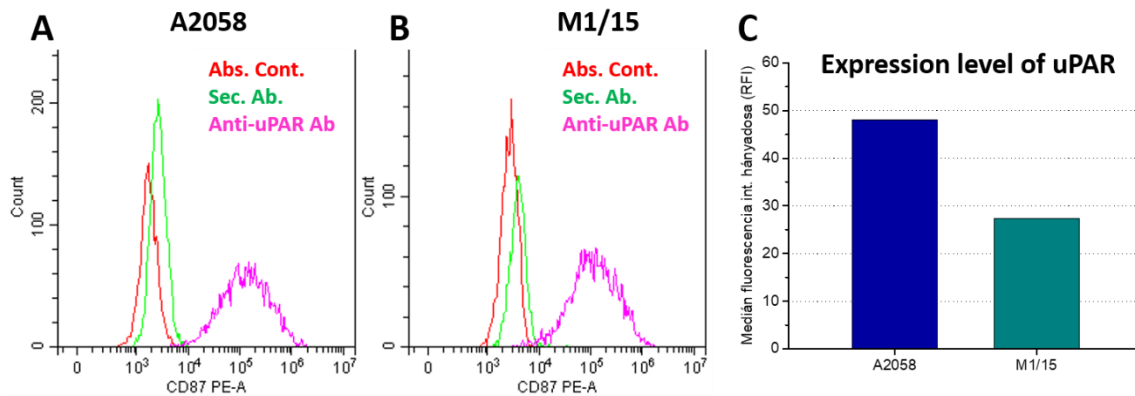
Figure 34. Expression of urokinase plasminogen activator receptor (uPAR or CD87) on A2058 (A) and M1/15 (B) model cells measured by CytoFLEX flow cytometer. For comparison of the expression level of uPAR on the melanoma cells (C) the median fluorescence intensity was used. RFI means ratio of median fluorescence intensity of CD87-labelled cells and median fluorescence intensity of cells labelled only with seconder antibody.

First, the peptides' effect on tumor cell adhesion and proliferation was investigated *via* impedimetry (xCELLigence SP) in a wide concentration range (0,1-100 µM). None of the peptides had significant influence on proliferation on A2058 cells; however, in case of M1/15 cells the [SRSSY]$_{cyclo}$ at the highest concentration (100 µM) seemed to reduce the cell viability.

H1, A6, WX-360 and [SRSSY]$_{cyclo}$ at 1 µM reduces notably the adhesion of A2058 cells both in short (5h) and long term (72h). Only the H1 peptide had a similar long-term adhesion decreasing effect in M1/15 cells. The rest of the peptides had no impact ([SRSSY]$_{cyclo}$) or the reducing effect (e.g. WX-360 and A6) on M1/15 cell adhesion was detected only in short term (5h). To further investigate in detail the effect of these four peptides on cell attachment, the cell morphological changes were measured in holographic microscope (Holomonitor M4).

For peptides WX-360 and H1 the decreased A2058 cell adhesion (impedance) was detected at 1 µM while cell spreading (area occupied by the cells) was also decreased in morphological studies. In the

case of [SRSSY]$_{cyclo}$, the area and volume of A2058 cells were significantly increased in holographic microscopic measurements. It is likely that for [SRSSY]$_{cyclo}$, the effect of volume change is the crucial step, not its effect on cell adhesion.

However, in M1/15 cells, no or opposite correlations were observed between the results of impedimetric and holographic microscopic measurements. It is possible that these peptides mediate their adhesion modulator effect by increasing or decreasing the distance between the cells and the electrode surface and not by influencing the contact area (spreading) of the attached cells.

It was clearly shown in the cell motion analysis that WX-360 and H1 had different effect on the two melanoma cells. WX-360 reduced the straight, direct migration of A2058 cells to the greatest extent, although the cells took a more sinuous path (**Figure 35. A-B**), while the motion of M1/15 cells was increased (Figure 3. A-B). That means M1/15 cells migrated further and took a more linear path.
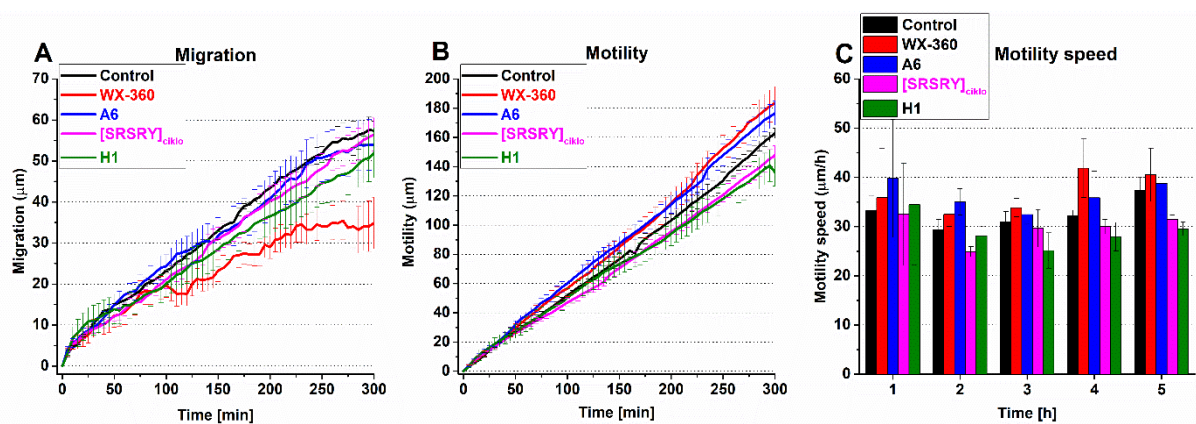
Figure 35. Effects of urokinase plasminogen activator receptor antagonist peptides on the migration (A), motility (B) and motility speed (C) of A2058 melanoma cells. Migration, motility and motility speed were investigated by HoloMonitor™ M4 holographic microscopy. Data shown in the figures represent averages ±SD values. Averages were calculated for 25 cell/group in 60 consecutive frames (time interval: 5 min).

In A2058 cells, H1 inhibited all parameters describing cell movement (motility: actual path, migration: shortest distance, migration speed) (**Figure 35. A-C**), but this peptide did not have any effect on the migration and motility of M1/15 cells (**Figure 36. A-C**). In both melanoma cells, A6 increased the motility (**Figure 35. B** and **Figure 36. B**), but the migration of the cells did not change significantly compared to the control (**Figure 35. A** and **Figure 36. A**). That means, the cells would rather crawl around than migrate far away. The [SRSSY]$_{cyclo}$ could also retain the M1/15 cells at the original site by reducing their migration (**Figure 36. A**).
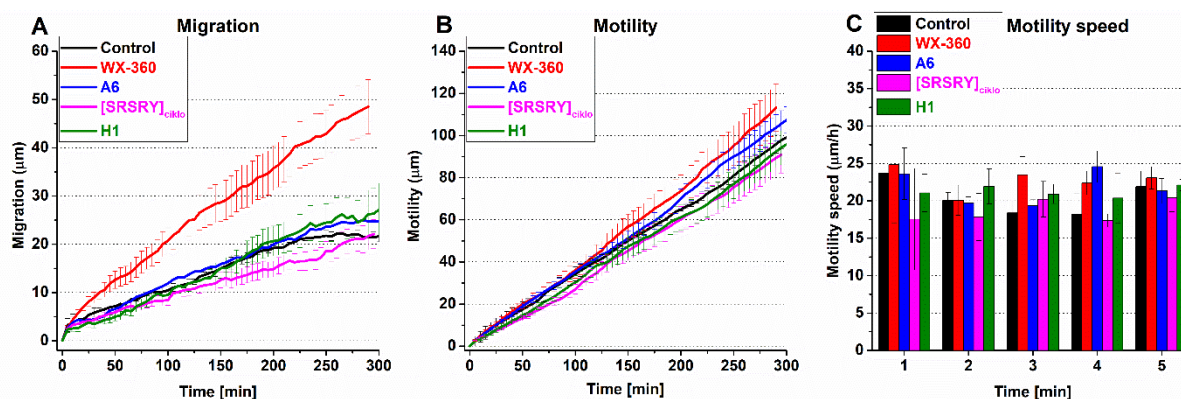
Figure 36. Effects of urokinase plasminogen activator antagonist peptides on the migration (A), motility (B) and motility speed (C) of M1/15 melanoma cells. Migration, motility and motility speed were investigated by HoloMonitor™ M4 holographic microscopy. Data shown in the figures represent averages ±SD values. Averages were calculated for 25 cell/group in 60 consecutive frames (time interval: 5 min).

In general, the cell adhesion modulatory effects of the peptides were less prominent in M1/15 cells than in case of A2058 cells. Morphological changes were correlated quite well with the impedimetric results only in case of A2058 cells. The effect of the peptides on cell movement proved to be cell dependent. H1, as an allosteric inhibitor of uPAR, could typically reduce the chance of A2058 dissemination by inhibiting their movement, while it had a more significant effect on the adhesion and the morphology of M1/15 cells. Although [SRSSY]$_{cyclo}$ interfering with one of the co-receptor of uPAR did not significantly reduce A2058 cell locomotion, it did notably alter the morphology and adhesion of this cell line; however, in M1/15 cells, rather the cell movement was affected. All in all, it is hypothesized that H1 and [SRSSY]$_{cyclo}$ could not serve melanoma cell spreading and dissemination, but by different mechanism.

Discrepancy in the effect of the peptides could be explained by the difference in the expression of uPAR (expression level of uPAR was higher in A2058 than M1/15) and its co-receptors (*e.g.* integrins, formyl-peptide receptor) on our model cells.

12. Optimization of mass spectrometry for Dau containing peptide drug conjugates

Daunorubicin was used for the development of a large number of peptide-drug conjugates in our laboratory that showed efficient antitumor activity not only in vitro, but also *in vivo*. Daunorubicin consists of an anthraquinone aglycon part and a daunosamine sugar moiety linked to the tetracycline by a glycosidic bond. Due to the complex structure of PDCs, tandem mass spectrometry is an indispensable tool for verification of the structure and purity of synthetic products. High sensitivity of mass spectrometers enables detailed analysis of PDCs structure and the changes thereof even at very low analyte concentrations. Mass spectrometry is widely used to determine the release of drugs from PDCs, and to identify their metabolites. In the case of anthracycline containing PDCs, however, mass

spectrometric analysis is hindered by the degradation of the compounds during electrospray ionization (ESI). ESI is a soft ionization technique, producing intact, singly or multiply protonated molecules from peptides. However, daunorubicin containing bioconjugates show significant in-source fragmentation under the commonly used experimental conditions, such as ESI ionization from slightly acidic solutions. 8 Spontaneous dissociation of the glycosidic bond in the ion source results in the appearance of intensive fragments with sugar loss, which hinders the mass spectrometric analysis significantly. Therefore, our aim was to investigate in detail the fragmentation properties of daunorubicin containing peptide conjugates, using energy-resolved tandem mass spectrometric (MS/MS) experiments.

In conclusion, the mass spectrometric analysis of daunorubicin containing peptide-conjugates is difficult due to the facile loss of the sugar moiety during ionization. The in-source fragmentation of the molecules results in complex mass spectra, which could lack peaks of important protonated PDC molecules in their intact forms. Fragmentation of this type of PDCs depends on several parameters. In addition to being dependent on instrument settings and solvent composition, fragment ion intensities and fragment ion types are dependent on structure. Our investigation verified that the MS/MS peak intensities and ratios of the sugar eliminated +1 or +2 charged product ions were strongly influenced by the amino acid chain length and the basicity of the sequence. These results could be used to predict mass spectrometric behaviour of these PDCs and could help in the evaluation of the mass spectrometric results as well as in the optimization of their MS detection [83].

"Overprotonation" can occur if daunomycin is linked to positively charged peptide carriers, like tuftsin derivatives. In these molecules, the high number of positive charges enhances the in-source fragmentation significantly, leading to complex mass spectra composed of mainly fragment ions. Therefore, we investigated different novel tuftsin-daunomycin conjugates (**Figure 37**.) to find an appropriate condition for mass spectrometric detection [84]. Our results showed that shifting the charge states to lower charges helped to keep ions intact. In this way, a clear spectrum could be obtained containing intact protonated molecules only. Shifting of the protonation states to lower charges could be achieved with the use of appropriate neutral volatile buffers and with tuning the ion source parameters.
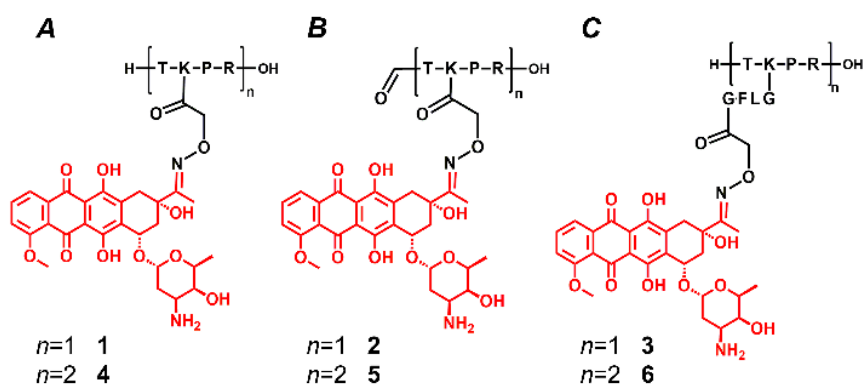
Figure 37. Schematic structure of the novel daunomycin-tuftsin bioconjugates

The novel daunomycin-tuftsin conjugates behaved as expected under the commonly used conditions, *i.e.*, a higher number of positively charged functional groups in the molecule indicated higher fragmentation (**Figure 38**.). Consequently, intact protonated ions were detected in lower amounts in the case of the free N-terminal containing conjugates, while formylation of the *N*-terminal (**2** and **5**) resulted in significantly lower fragmentation. We also found that enhanced distance between the sugar moiety and the positively charged peptide backbone (incorporation of the GFLG spacer) decreased the fragmentation. According to these observations, we can conclude that special structural modifications can influence (enhance or decrease) the gas-phase stability of daunomycin, *i.e.*, affect the split of the sugar moiety, but these effects are rather small. An overview of these data is represented in **Figure 39.**
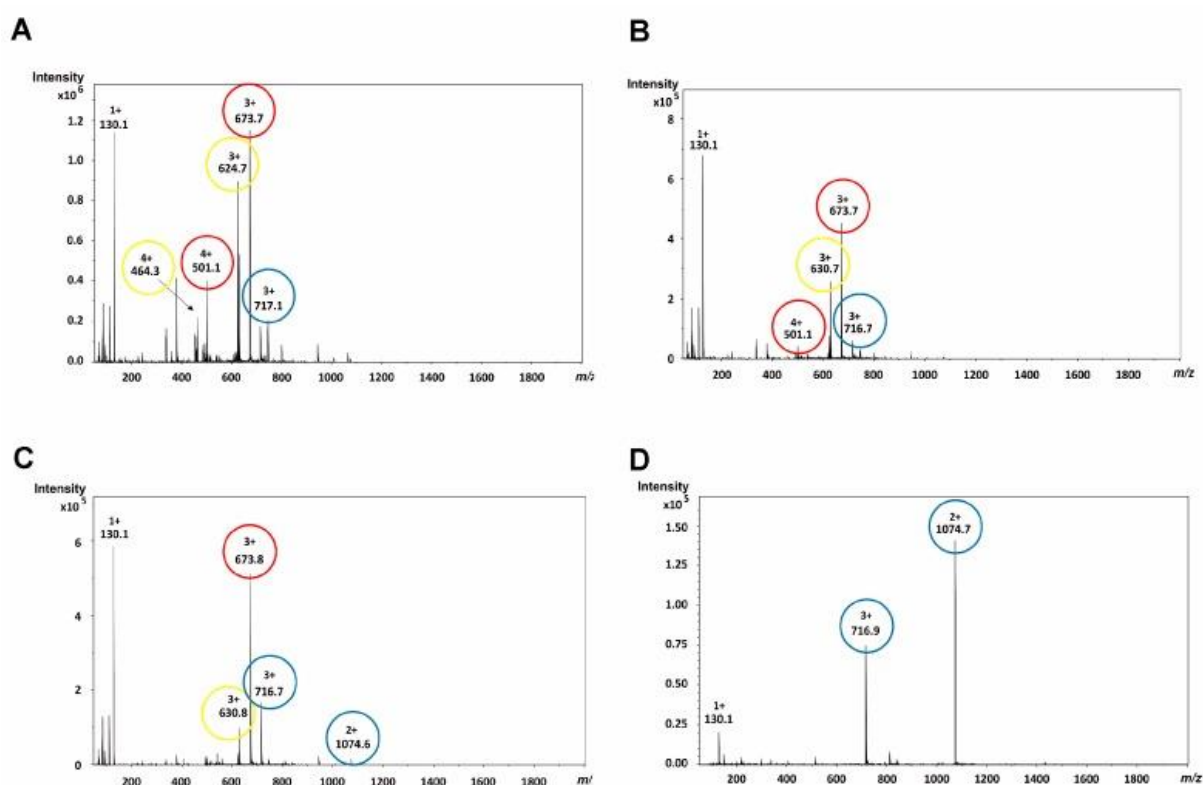
Figure 38. ESI-MS spectra of conjugate 4 (A) under the commonly used ion source parameters (136 V capillary exit potential); (B) using reduced capillary exit potential (5 V); (C) in non-acidic solvent mixture (acetonitrile-water 50:50% v/v; 5 V capillary exit potential); (D) measured in 50 mM NH4OAc buffer (pH = 6.7, diluted with acetonitrile 50:50% v/v; 5 V capillary exit potential). Blue circles are used to label intact protonated molecules, yellow and red circles label protonated fragment ions with one and two sugar losses, respectively. Charge states and *m/z* values of the protonated molecules are shown in the Figure.

We hypothesized that optimized ion source parameters or appropriate solvent mixtures used for the ionization would reduce the in-source fragmentation of the samples. Hence, we changed the capillary exit potential, and we could show that the reduction of this mass spectrometric parameter could slightly decrease the fragmentation. In the case of compound 2, this modification in the mass spectrometric conditions resulted in a significantly improved spectrum, in which intact protonated ions were detected

as base peaks (97%, Figure 4). The spontaneous dissociation of the glycosidic bond was facilitated by the highly charged peptide chain, therefore, shifting the charge states to lower charges could help to keep ions intact during ESI-MS analysis. Hence, application of neutral or slightly basic volatile buffers for the ESI-MS measurements could significantly reduce the fragmentation of the analyte and, therefore, reduce the amount of the sugar lost ions in the spectra. In our experiments, the most appropriate buffer for suppressed fragmentation was ammonium acetate (pH 6.7). NH_4OAc buffer in acetonitrile combined with low capillary exit potential (5 V) could significantly reduce the charge states of various daunomycin-tuftsin conjugates and decrease their in-source fragmentation (**Figure 39**). In conclusion, not only the settings of the mass spectrometer but also the structure of the daunomycin-tuftsin conjugates had a high impact on the ESI-MS spectra. Though structural changes can assist the reduction of the fragmentation, overprotonation can only be suppressed with appropriate solvents and optimized mass spectrometric settings. These conditions can be useful in the analysis of anthracycline-containing bioconjugates in general, to obtain mass spectra comprising intact protonated molecules only.

.
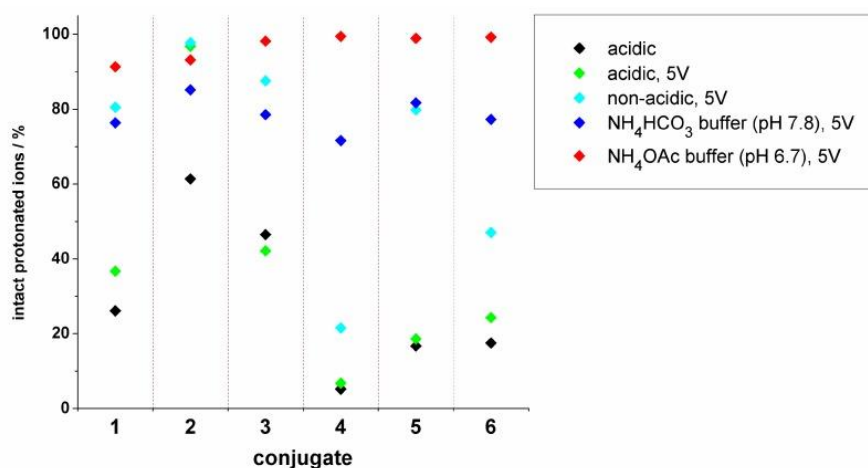
Figure 39. The intensity of the intact protonated ions (%) in the case of novel tuftsin-daunomycin conjugates under various conditions. The capillary exit potential, the solvents, and the pH were modified systematically.

In a further study, we comprehensively compared the performance of common fragmentation techniques, such as higher energy collisional dissociation (HCD), electron transfer dissociation (ETD), electron-transfer higher energy collisional dissociation (EThcD) and matrix-assisted laser desorption/ionization–tandem time-of-flight (MALDI-TOF/TOF) activation methods for the structural identification of synthetic daunomycin-peptide conjugates by high-resolution tandem mass spectrometry [85]. In this study the Angiopep-2 – Dau conjugates and α-MSH peptide derivatie – Dau conjugates (**Figure 40**) were applied in which the drug was attached in different position of the peptide chain.

We found that daunomycin-related fragmentation is still the major fragmentation pathway using the most common fragmentation techniques, namely, HCD, ETD and EThcD. Conjugation of the peptides with daunomycin increased both the molecular weight and the gas-phase basicity of the conjugates. Such

chemical modification greatly influenced the fragmentation efficiency of the bioconjugates, higher energies and higher charge states were required to "mobilize" the protons and facilitate charge-directed backbone cleavages than for the unmodified peptides. Based on these results, an appropriate selection of the precursor charge state and HCD energy can provide a complete sequence coverage and facilitate the conjugation site assignment. We have also shown that peptide backbone fragmentation was inhibited in these conjugates using ETD or EThcD methods, most possibly due to the "electron predator" effect of the daunomycin. MALDI-TOF/TOF analysis of daunomycin bioconjugates yielded structural information about the targeting peptide and allowed discrimination between different drug conjugation sites even in the case of large and complex molecules. When used along with collisional activation, the MALDI-MS/MS spectra of the conjugates were dominated by fragments related to characteristic peptide sequences aside from the facile sugar and daunomycin lost fragments. The presence of intense a-ions, which corresponded to the peptide backbone cleavage at or within the vicinity of Lys residues that contained the modifications, improved the localization of side chain conjugations. However, MALDI-TOF/TOF provided an incomplete sequence coverage. We envision that MALDI-CID-MS/MS will be the method of choice for structure identification and comprehensive characterization of peptide-drug conjugates containing anthraquinone, quinoline or other polyheterocyclic analogs as payloads.
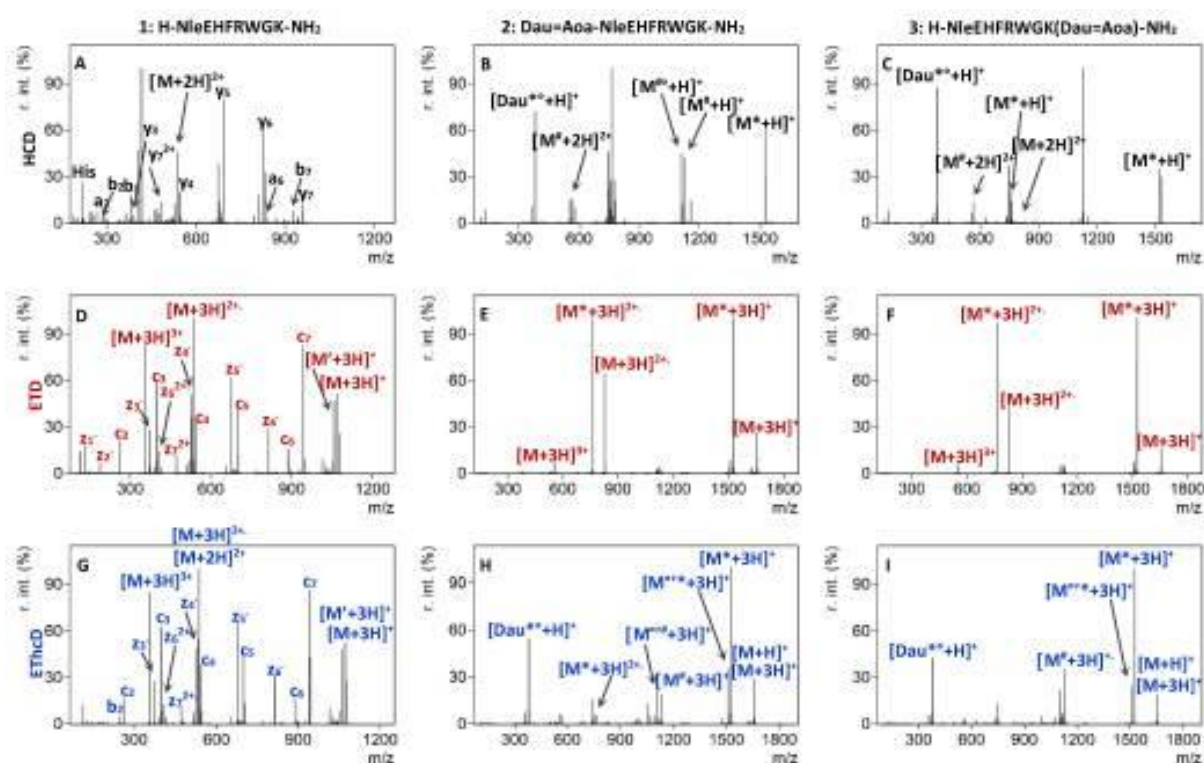

Figure 40. HCD MS/MS spectra of the doubly protonated peptide 1 (A) at 30% NCE and conjugates 2 (B), and 3 (C) at 20% NCE. ETD MS/MS spectra of the triply protonated 1 (D), 2 (E), and 3 (F). EThcD MS/MS spectra of the triply protonated 1 (G) at 10% NCE, and 2 (H) and 3 (I) at 40% NCE. Neutral losses are depicted as follows: * = sugar, ' = NH$_3$, = H$_2$O, # = Dau + sugar.

## 13. Formulation to improve the bioavailability of drug molecules

Cyclodextrins (CDs) are cyclic, water-soluble oligosaccharides commonly constituted by 6 to 8 α-D-glucopyranose units. The most appealing characteristic of CDs is that they have a relatively lipophilic central cavity which readily forms an inclusion complex with a lipophilic compound or moiety, meanwhile the hydrophilic outer surface of the CD molecule grants a highly water-soluble complex [86]. Moreover, CDs are also used to improve the stability of the complexed molecules [87]. For the reasons described, currently there are at least 50 FDA-approved pharmaceutical products containing CDs as excipients [87]. Modified CDs, like 2-hydroxypropyl-β-CD (HP-β-CD), are often preferred for pharmaceutical applications as they have increased water-solubility and they are suitable for parenteral administration due to their low molecular weight and low toxicity [88].

Electrospinning (ES) is considered to be a promising alternative to freeze-drying as ES is a continuous and energy-efficient process with gentle and instant solvent evaporation at room temperature. The process produces (drug-loaded) nano or microfibers from viscous polymer or from CD solutions *via* high electric field, and the resulting fibers have a large surface area providing fast dissolution [90]. ES has been a popular method to produce drug delivery systems for various application areas *e.g.* biopharmaceutical formulations [91]. However, there are some challenges associated with the ES technology. Scaled-up production of fibers is not straightforward and the use of high voltage can pose a safety concern [92.], however, with proper equipment design it can be handled. Moreover, sterile manufacturing is a challenge, but it can be overcome similarly to spray drying. Besides, most polymer fibers have low friability, which can make final dosage form development challenging [93].

In this work a new solid DOX-HP-β-CD formulation was prepared in a scaled-up manner by high-speed electrospinning [94]. This formulation could be applied as an *i.v.* bolus dosage form, as fibers containing one dose of DOX (100 mg) was easily dissolvable in 1.5 mL water resulting in a particle free solution. The DOX concentration in the reconstituted solution was 66.7mg/(mL solvent), which is nearly 7 times higher than the currently marketed formulations (*e.g.* Doxycycline for Injection by Mylan®) after reconstitution. This new *i.v.* bolus DOX-HP-β-CD dosage form could be useful in rapid onset infections (*e.g.* anthrax, plague), when fast administration of DOX can be lifesaving. Furthermore, our experiments proved that HSES is a viable continuous alternative to the batch freeze-drying technology (**Figure 41** and **Figure 42.**). The high productivity (~80 g/h) of the used HSES technology creates the opportunity to produce approx. 2200 doses of *i.v.* bolus applicable DOX per day, thus fulfilling the requirements of the pharmaceutical industry.
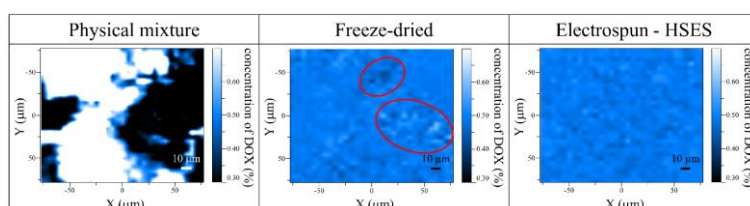
Figure 41. Homogeneity study of the physical mixture of DOX and HP-β-CD, the freeze-dried DOX-HP-β-CDand the electrospun (HSES) DOX-HP-β-CD complexes.
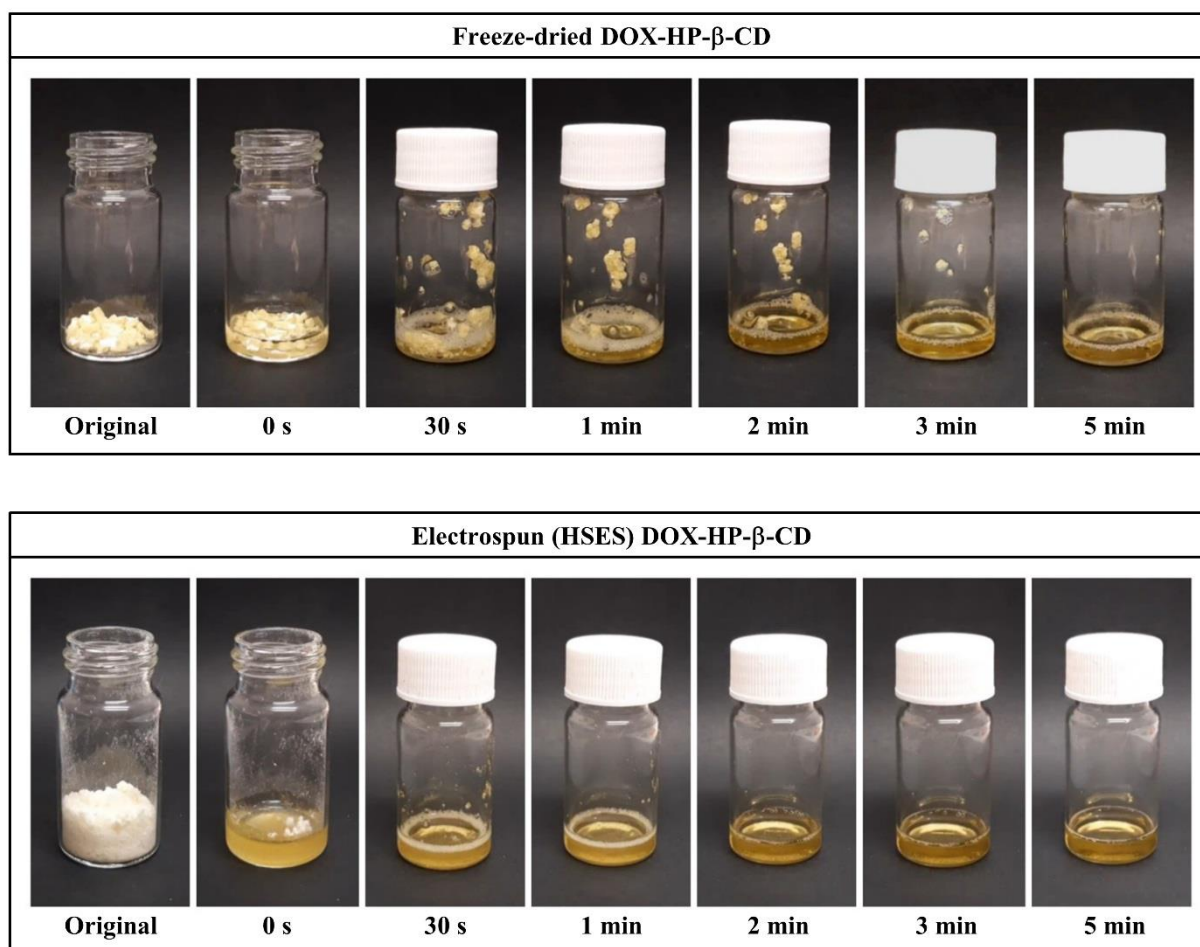
Figure 42. Images of the dissolution test of electrospun (HSES) and the freeze-dried DOX-HP-β-CD complex

Curcuminoids (CUs) of antitumor and various other potential biological activities have extremely low water solubility and bioavailability therefore, special formulation was elaborated [95]. New fast dissolving reconstitution dosage forms of four CUs were prepared as fibrous form of 2-hydroxypropyl-β-cyclodextin (HP-β-CD). In the electrospinning process HP-β-CD could act both as solubilizer and fiber-forming agent. The solubilization efficiency of the CU-HP-β-CD systems was determined with phase-solubility measurements. The electrospun CUs were amorphous and uniformly distributed in the fibers according to XRD analysis and Raman mappings. The fibrous final products had fast (<5 min) and complete dissolution. In typical iv. infusion reconstitution volume (20 mL) fibers containing 40–80 mg of CU could be dissolved, which is similar to the currently proposed dose (<120 mg/m^2). The in vitro cytostatic effect data showed that the antitumor activity of the CU-HP-β-CD complexes was similar or better compared to the free APIs.

In this work, a new solid CU-HP-β-CD formulation was prepared with lab-scale and pilot-scale HSES [96]. The applicability of the new formulation was shown with four different CUs. The electrospun CUs were amorphous and uniformly distributed in the fibers according to XRD analysis and Raman mappings. The fibers could be dissolved in water in a short time frame resulting in a particle-free

solution. In typical *iv.* infusion reconstitution volume (20 mL) 40–80 mg of CU could be achieved, which is similar to the currently proposed dose (<120 mg/m^2). The *in vitro* cytostatic effect data showed that the antitumor activity of the CU-HP-β-CD complexes was similar with the free APIs or even better. Moreover, the electrospun samples were solved solely in water during the *in vitro* evaluation, while the free APIs were solved with added DMSO (adequate stock solution concentration is not achievable without DMSO) which could further increase the cytostatic effect. However, one complex ((1E,6E)-1,7-bis(3-hydroxyphenyl)hepta-1,6-diene-3,5-dione) had a significantly lower cytostatic effect, than the free API, thus indicating that aryl moiety-HP-β-CD interaction could inhibit the cytostatic effect of the CUs. The results showed that there is a lot of potential in the presented CU-HP-β-CD complex systems in cancer therapy. Moreover, the HSES technology combined with the HP-β-CD complex system have the potential to bridge the gap in the CUs *iv.* application, due to it has high production rate and the applied HP-β-CD is a safe, FDA approved excipient (even in *iv.* administration form).

In the next study [97], the solubility of EGFR specific peptide-drug conjugates was improved by the attachment of PEG or HbPG (hyperbranched polyglycerol [98]) (**Figure 43.**).
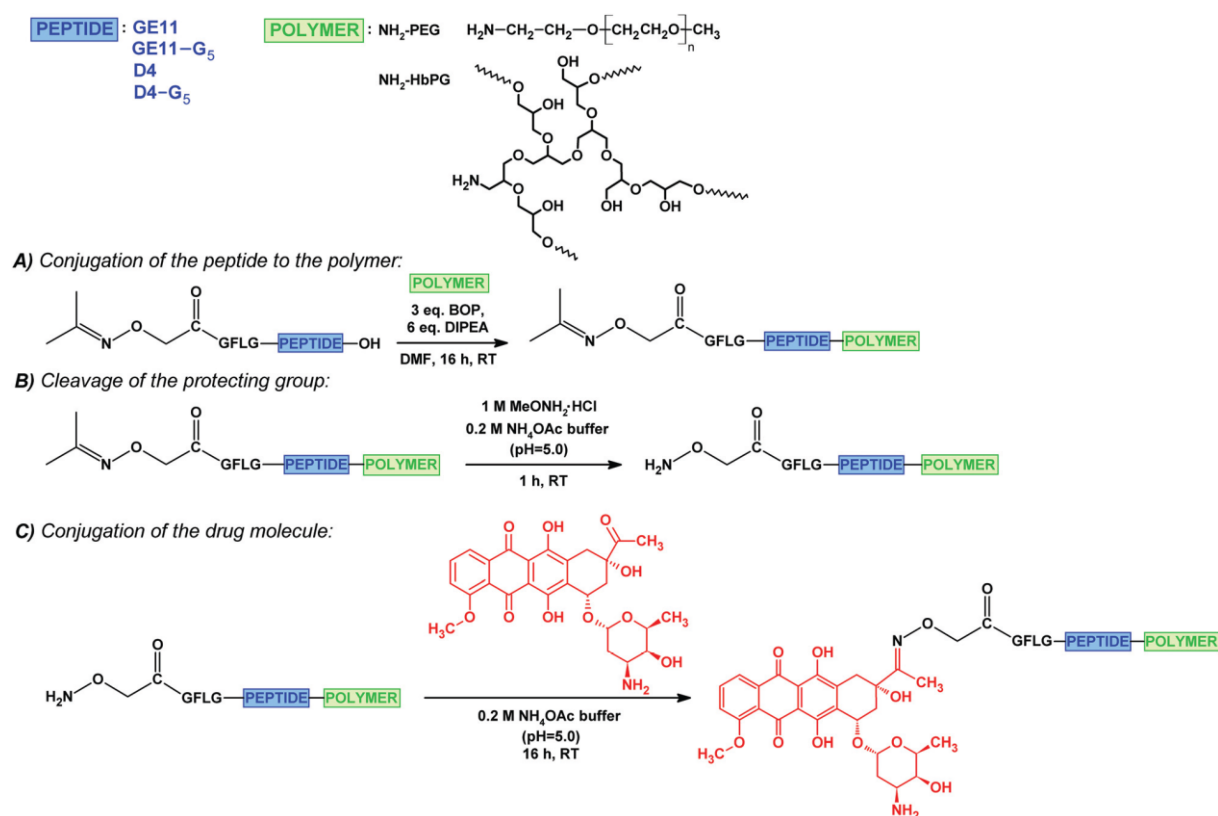
Figure 43. Synthesis of the drug–peptide–polymer conjugates: the conjugation of the isopropylidene protected aminooxyacetylated peptide to the aminomonofunctional
polymer (PEG or HbPG) (A); cleavage of the isopropylidene protecting group (B); conjugation of daunomycin via oxime linkage (C).

The epidermal growth factor receptor (EGFR) is a widely used target receptor for cancer therapy. In this work, GE11 ((YHWYGYTPQNVI) [99] and D4 (LARLLT) [100] EGFR targeting peptides containing drug conjugates with systematic structural variations were prepared and investigated. As observed, the cathepsin B labile spacer (GFLG), which was incorporated between the targeting peptide and the daunomycin to ensure the efficient release of the active metabolite, highly increases the hydrophobicity of the conjugates. As demonstrated, the solubility problem of these conjugates can be solved by hydrophilic polymer coupling, not only by using the well-known PEG but also by using the amino-monofunctional HbPG. To the best of our knowledge, 1:1 covalent peptide–polymer conjugates with well-defined monofunctional HbPG have been reported by us for the first time. The results of the *in vitro* cell viability and cellular uptake measurements on HT-29 human colon adenocarcinoma cells prove that the HbPG and the PEG highly influenced the biological activity of the drug–peptide–polymer conjugates. In both peptide conjugate series, one GE11 and one D4 targeting peptide-based conjugate were found with outstanding cellular uptake and cytotoxicity values, namely Dau=Aoa–GFLG–GE11–PEG and Dau=Aoa–GFLG–D4–G5–HbPG (**Table 11**.).

Table 11. Calculated IC50 values of the daunomycin-peptide-polymer conjugates after 48 hours and the critical aggregation concentration (cac) of the conjugates, the size (d) and the dispersity (PDI) of the nanoparticles determined by DLS measurement.

	IC_{50} (μM)	d (nm)	PDI	cac (μM)
Dau=Aoa-GFLG-GE11-PEG	1.2	370.0	0.082	28.6 ± 4.4
Dau=Aoa-GFLG-GE11-G₅-PEG	9.1	171.8	0.137	9.3 ± 0.9
Dau=Aoa-GFLG-GE11-HbPG	9.3	83.8	0.144	16.6 ± 1.6
Dau=Aoa-GFLG-GE11-G₅-HbPG	6.0	52.3	0.092	20.2 ± 2.9
Dau=Aoa-GFLG-D4-PEG	5.1	189.3	0.130	16.1 ± 1.3
Dau=Aoa-GFLG-D4-G₅-PEG	13.5	157.4	0.076	56.9 ± 3.2
Dau=Aoa-GFLG-D4-HbPG	>50.0	76.5	0.057	6.4 ± 1.2
Dau=Aoa-GFLG-D4-G₅-HbPG	3.8	71.3	0.042	13.4 ± 0.5

Based on the performed DLS measurements, the conjugates have amphiphilic character and all conjugates aggregate above a specific concentration (cac) which leads to nanoparticle formation with 60–370 nm size, which depends on the composition of the conjugates. In general, the size of the HbPG containing conjugate nanoparticles is lower than that of the PEG analogues. This is related to the lower hydrodynamic volume of the HbPG, which has a compact hyperbranched structure in contrast to the linear PEG. The incorporation of the pentaglycine (G5) spacer between the targeting peptide and the polymer influences the philicity and also increases the accessibility of the peptide segment. It was found that the G5 spacer influences not only the biological activity (internalization and toxicity) but also the aggregation. This latter property of the drug–peptide–polymer conjugates is also affected by the steric

hindrance of the hydrophilic polymer. Hence, it can be generally concluded that the investigation of the colloidal properties, such as self-aggregation behaviour and nanoparticle formation, is necessary for the better understanding of the biological activity of bioconjugates with amphiphilic character, which can reveal the structure–activity relationship of amphiphilic drug–peptide–polymer conjugates for tumor targeting. Our findings strongly indicate that the solubilization or apparent solubilization of drugs or bioconjugates is not a sufficient criterion for increased bioactivity. The formation of nanoparticle aggregates may hinder the targeting moiety for the high extent of receptor binding, on the one hand. On the other hand, the enzyme labile spacer may also be blocked in such nanoparticles. In order to overcome these difficulties, the structure of the receptor binding moiety and the solubilizing polymer must be well aligned for highly efficient drug targeting. According to our results, the PEG is suitable for longer targeting peptides (*e.g.* GE11), but the G5 spacer is not suitable irrespective of the length of the peptide because it may decrease the biological effect by increasing the flexibility of the polymer and shading of the targeting moiety. In contrast, the use of the hydrophilic hyperbranched polyglycerol (HbPG) is advantageous for short targeting peptides (*e.g.* D4) but only with a G5 spacer, which provides accessibility of the peptide for receptor binding and cellular uptake resulting in outstanding cytotoxicity.

14. Development of new drug derivatives

A new anthracycline derivative 2-pyrrolino-daunorubicin was previously developed previously in our laboratory. We provided a new synthetic route for the high scale efficient synthesis of the drug. Unfortunately, this very cytotoxic compound (2-3 magnitude higher cytotoxicity than daunorubicin or doxorubicin) was not suitable for conjugation of peptides. Therefore, this drug molecule was used in liposomal form LyPyDau, that showed very efficient *in vivo* effect in mice. Complete tumor regression was detected on breast cancer bearing mice. Therefore, the compound was patented as highly efficient nanodrug for cancer treatment [101]. The patent has been published recently. Moreover, new anthracycline derivatives have been developed that might be suitable for conjugation to peptides. The synthesis of the conjugates and study of their *in vitro* and *in vivo* anticancer activity are in progress. According to the results, the compounds might be patented, too, therefore their structures cannot yet be presented.

15. Publication

27 manuscripts (mainly D1 and Q1 articles) and 7 Symposium Proceedings have been published. However, our results and some ongoing experiments predestinate at least 8 further publications from the summarized topics in near future. These results were presented in different conferences during the last years. Four PhD thesis were done and four more will be finished between 2023-2025 that present the results summarized above. Several BSc. and MSc. thesis and thesis for Student's Scientific Competition were also made.

16. Future and perspectives

Peptide based drug targeting is still a hot topic. The collected results show that many potential homing peptides are needed for the personalized tumor therapy. Therefore, we believe that our results provide good evidence for the development of efficient drug candidates for targeted tumor therapy in the future. However, we can conclude that this therapeutic approach will be highly efficient only when the resistant tumor cells (*e.g.* cancer stem cells) could be eliminated, too, that have responsibility for the cancer relapse. For this purpose, we started to focus on the development of homing peptides that are suitable to target drug molecules efficiently to cancer stem cells and other type of resistant cancer cells.

16. References

1. **Vrettos E, Mező G, Tzakos A.** *Beilstein J Org Chem* **14: 930-954 (2018)**

2. Fosgerau K, Hoffmann T. *Drug Discov Today* 20: 122-128 (2015)

3. Hagimori M, Fuchigami Y, Kawakami S. *Chem Pharm Bull* 65: 618-624 (2017)

4. Raibaut L, Mahdi OE, Melnyk O. Topics in Current Chemistry (Springer: Cham, Switzerland) pp. 103-154, (2014)

5. Malins LR, Payne RJ. *Curr Opin Chem Biol* 22: 70-78 (2014)

6. Kapoor P, Singh H, Gautam A, Chaudhary K, Kumar R, Raghava GP. PLoS One 7: e35187 (2012)

7. Mező G, Manea M. *Expert Opin Drug Deliv* 7: 79-96 (2010)

8. Hyvonen M, Laakkonen P. *Methods Mol Biol* 1324: 205e222 (2015)

9. Tugyi R, Uray K, Iván D, Fellinger E, Perkins A, Hudecz F. *Proc Natl Acad Sci USA* 102: 413-418 (2005)

10. Gentilucci L, De Marco R, Cerisoli L. *Curr Pharm Design* 16: 3185-3203 (2010)

11. Soto, C.; Adessi, C. *Curr Med Chem* 9: 963-978 (2002)

12. Pappa EV, Zompra AA, Diamantopoulou Z, Spyranti Z, Pairas G, Lamari FN, Katsoris P, Spyroulias GA, Cordopatis P. *Biopolymers* 98: 5255-5234 (2012)

13. **Schuster S, Biri-Kovács B, Szeder B, Farkas V, Buday L, Szabó Z, Halmos G, Mező G.** *Beilstein J Org Chem* **14: 756-771 (2018)**

14. **Schuster S, Biri-Kovács B, Szeder B, Buday L, Gardi J, Szabó Z, Halmos G, Mező G.** *Pharmaceutics* **10: 223 (2018)**

15. **Randelović I, Schuster S, Kapuvári B, Fossati G, Steinkühler C, Mező G, Tóvári J.** *Int J Mol Sci* **20: 4763 (2019)**

16. **Schuster S, Juhász É, Halmos G, Neundorf I, Gennari C, Mező G.** *Int J Mol Sci* **23: 5071 (2022)**

17. Murányi J, Gyulavári P, Varga A, Bökönyi G, Tanai H, Vántus T, Pap D, Ludányi K, Mező G, Kéri G. *J Pept Sci* 22: 552-560 (2016)

18. Nomoto T, Nishiyama N. *In Photochemistry for Biomedical Applications* (Ito Y. Ed.; Springer: Singapore) pp 301-313 (2018)

19. **Pethő L, Murányi J, Pénzes K, Gurbi B, Brauswetter D, Halmos G, Csík G, Mező G.** *Int J Mol Sci* **20: 5027 (2019)**

20. Zhang J, Cui X, Yan Y, Li M, Yang Y, Wang J, Zhang J. *Am J Transl Res* 8: 2862-2875 (2016)

21. **Polgár L, Lajkó E, Soós P, Láng O, Manea M, Merkely B, Mező G, Kőhidai L.** *Beilstein J Org Chem* **14: 1583-1594 (2018)**

22. Hegedüs R, Manea M, Orbán E, Szabó I, Kiss E, Sipos E, Halmos G, Mező G. *Eur J Med Chem* 56: 155-165 (2012)

23. **Lajkó E, Hegedüs R, Mező G, Kőhidai L.** *Int J Mol Sci* **20: 4421 (2019)**

24. **Lajkó E, Spring S, Hegedüs R, Biri-Kovács B, Ingebrandt S, Mező G, Kőhidai L.** *Beilstein J Org Chem* **14: 2495-2509 (2018)**

25. Vincent A, Herman J, Schulick R, Hruban RH, Goggins M. *Lancet* 378: 607-620 (2011)

26. Siegel RL, Miller KD, Jemal A . *CA Cancer J Clin* 70: 7-30 (2018)

27. Hidalgo M. *N Engl J Med* 362: 1605-1617 (2010)

28. Zhang L, Sanagapalli S, Stoita A. *World J. Gastroenterol* 24: 2047-2060 (2018)

29. Carraway R, Leeman SE. *J Biol Chem* 248: 6854-6861 (1973)

30. Gilbert JA, McCormick DJ, Pfenning MA, Kanba KS, Enloe LJ, Moore A, Richelson E. *Biochem Pharm* 38: 3377-3382 (1989)

31. Gilbert JA, Richelson E. *Eur J Pharmacol* 99: 245-246 (1984)

32. Carraway RE, Plona AM. *Peptides* 27: 2445-2460 (2006)

33. **Dókus LE, Lajkó E, Ranđelović I, Vári-Mező D, Vári B, Borbély A, Tóvári J, Kőhidai L, Mező G. *Int J Mol Sci* under submission (2022)**

34. Majumdar S, Siahaan TJ. *Med Res Rev* 32: 637-658 (2012)

35. Jensen RT, Battey JF, Spindel ER, Benya RV. *Pharmacol Rev* 60: 1-42 (2008)

36. Begum AA, Wan Y, Toth I, Moyle PM. *Bioorg Med Chem* 26: 516-526 (2018)

37. Schroeder RPJ, Müller C, Reneman S, Melis ML, Breeman WAP, de Blois E, Bangma CH, Krenning EP, van Weerden WM, de Jong M. *Eur J Nucl Med Mol Imaging* 37: 1386-1396 (2010)

38. Nock BA, Kaloudi A, Lymperis E, Giarika A, Kulkarni HR, Klette I, Singh A, Krenning EP, de Jong M, Maina T, et al. *J Nucl Med* 58: 75-80 (2017)

39. **Gomena J, Vári B, Oláh-Szabó R, Biri-Kovács B, Bősze S, Borbély A, Tóvári J, Mező G. *Int J Mol Sci* under publication (2022)**

40. Curnis F, Arrigoni G, Sacchi A, Fischetti L, Arap W, Pasqualini R, et al. *Cancer Res* 62: 867-874 (2002)

41. Healy JM, Murayama O, Maeda T, Yoshino K, Sekiguchi K, Kikuchi M. *Biochemistry* 34: 3948-3955 (1995)

42. Enyedi KN, Czajlik A, Knapp K, Láng A, Majer Zs, Lajkó E, Kőhidai L, Perczel A, Mező G. *J Med Chem* 58: 1806-1817 (2015)

43. **Enyedi KN, Tóth S, Szakács G, Mező G. *PLoS One* 12: e0178632 (2017)**

44. Kapuvári B, Hegedűs R, Schulcz Á, Manea M, Tóvári J, Gacs A, Vincze B, Mező G. *Invest New Drugs* 34: 416-423 (2016)

45. **Tripodi AAP, Tóth S, Enyedi KN, Schlosser G, Szakács G, Mező G. *Beilstein J Org Chem* 14: 911-918 (2018)**

46. **Tripodi AAP, Ranđelović I, Biri-Kovács B, Szeder B, Mező G, Tóvári J. *Pathol Oncol Res* 26: 1879-1892 (2020)**

47. Máté G, Kertész I, Enyedi KN, Mező G, Angyal J, Vasas N, Kis A, Szabó É, Emri M, Bíró T, Galuska L, Trencsényi G. *Eur J Pharm Sci* 69: 61-71 (2015)

48. **Szabó JP, Denes N, Arató V, Racz S, Kis A, Opposits G, Kepes Z, Hajdu I, Jószai I, Emri M, Kertész I, Mező G, Trencsényi G. *In Vivo* 36: 1667-1675 (2022)**

49. **Kis A, Szabó JP, Dénes N, Vágner A, Nagy G, Garai I, Fekete A, Szikra D, Hajdu I, Matolay O, Méhes G, Mező G, Kertész I, Trencsényi G. *Biomed Res Int* 2020: 4952372 (2020)**

50. **Kis A, Dénes N, Szabó JP, Arató V, Jószai I, Enyedi KN, Lakatos S, Garai I, Mező G, Kertész I, Trencsényi G. *Int J Pharm* 589: 119881 (2020)**

51. **Farkasinszky G, Dénes N, Rácz S, Kis A, Péliné JS, Opposits G, Veres G, Balkay L, Kertész I, Mező G, Hunyadi J, Trencsényi G. *In Vivo* 36: 657-666 (2022)**

52. **Dénes N, Kis A, Szabó JP, Jószai I, Hajdu I, Arató V, Enyedi KN, Mező G, Hunyadi J, Trencsényi G, Kertész I. *Appl Radiat Isot* 174: 109778 (2021)**

53. **Kiss K, Biri-Kovács B, Szabó R, Ranđelović I, Enyedi KN, Schlosser G, Orosz Á, Kapuvári B, Tóvári J, Mező G.** *Eur J Med Chem* **176: 105-116 (2019)**

54. Zhang B, Yan Y, Shen Q, Ma D, Huang L, Cai X, Tan S. *Mater Sci Eng C Mater Biol Appl* 79: 185-190 (2017)

55. Fourie AM, Sambrook JF, Gething MJ. *J Biol Chem* 269: 30470-30478 (1994)

56. Braun KP, Pavlovich JG, Jones DR, Peterson CM. Alcohol Clin Exp Res 21: 40-43 (1997)

57. Basu A, Chakrabarti A. *J Proteomics* 128: 469-475 (2015)

58. Shevtsov M, Huile G, Multhoff G. *Philos Trans R Soc Lond B Biol Sci* 373: 20160526 (2018)

59. Escrivá-De-Romaní S, Arumí M, Bellet M, Saura C. *Breast* 39: 80-88 (2018)

60. Karasseva NG; Glinsky VV, Chen NX, Komatireddy R, Quinn TP. *Protein J* 21: 287-296 (2002)

61. Geng L, Wang Z, Jia X, Han Q, Xiang Z, Li D, Yang X, Zhang D, Bu X, Wang W, et al. *Theranostics* 6: 1261-1273 (2016)

62. **Biri-Kovács B, Adorján A, Szabó I, Szeder B, Bősze S, Mező G.** *Biomolecules* **10: 183 (2020)**

63. Joyce JA, Laakkonen P, Bernasconi M, Bergers G, Ruoslahti E, Hanahan D. *Cancer Cell* 4: 393-403 (2003)

64. **Dókus LE, Lajkó E, Randelović I, Mező D, Schlosser G, Kőhidai L, Tóvári J, Mező G.** *Pharmaceutics* **12: 576 (2020)**

65. **Vári B, Dókus L, Borbély A, Gaál A, Vári-Mező D, Randelović I, Varga Z, Szoboszlai N, Mező G, Tóvári J.** *Drug Delivery* **submitted (2022)**

66. Demeule M, Régina A, Ché C, Poirier J, Nguyen T, Gabathuler R, Castaigne J-P, Béliveau R. *J Pharmacol Exp Ther* 324: 1064–1072 (2008)

67. Régina A, Demeule M, Ché C, Lavallée I, Poirier J, Gabathuler R, Béliveau R, Castaigne J-P. *Br J Pharmacol* 155: 185-197 (2008)

68. Ché C, Yang G, Thiot C, Lacoste MC, Currie JC, Demeule M, Régina A, Béliveau R, Castaigne J-P *J Med Chem* 53: 2814-2824 (2010)

69. **Pethő L, Oláh-Szabó R, Mező G.** *Proceedings of the 36th European Peptide Symposium* **pp. 147-150 (2022)**

70. **Pethő L, Oláh-Szabó R, Mező G.** *J Control Releas* **under submission (2022)**

71. Iacob G, Dinca EB. *J Med Life* 2: 386-393 (2009)

72. Debinski W, Gibo DM, Hulet SW, Connor JR, Gillespie GY. *Clin Cancer Res* 5: 985-990 (1999)

73. Sharma P, Debinski W. *Int J Mol Sci* 19: 3326 (2018)

74. Pandya H, Gibo DM, Garg S, Kridel S, Debinski W. *Neuro-Oncol* 14: 6-18 (2012)

75. Mező G, Manea M, Jakab A, Kapuvári B, Bősze S, Schlosser G, Przybylski M, Hudecz F. *J Pept Sci* 10:701-713 (2004)

76. Moroder L. *J Pept Sci* 11: 187-214 (2005)

77. Yamada Y, Kanayama S, Ito F, Kurita N, Kobayashi H. *Biomedical Reports* 7: 221-225 (2017)

78. Sato S, Kopitz C, Schmalix WA, Muehlenweg B, Kessler H, Schmitt M, Krüger A, Magdolen V. *FEBS Lett* 528: 212-216 (2002)

79. Skovgaard D, Persson M, Kjaer A. Urokinase *PET Clin* 12: 311-319 (2017)

80. Pollaro L, Diderich P, Angelini A, Bellotto S, Wegner H, Heinis C. *Anal Biochem* 427: 18-20 (2012)

81. Finlayson M. *Front Immunol* 135: 1-8 (2015)

82. Yousif AM, Ingangi V, Merlino F, Brancaccio D, Minopoli M, Bellavita R, Novellino E, Carriero MV, Carotenuto A, Grieco P. *Eur J Med Chem* 143: 348-360 (2018)

83. **Al-Majidi M, Szabó D, Dókus L, Steckel A, Mező G, Schlosser G.** *J Mass Spectrom* **55: e4641 (2020)**

84. **Pethő L, Mező G, Schlosser G.** *Molecules* **24: 2981 (2019)**

85. **Borbély A, Pethő L, Szabó I, Al-Majidi M, Steckel A, Nagy T, Kéki S, Kalló G, Csősz É, Mező G, Schlosser G.** *Int J Mol Sci* **22: 1648 (2021)**

86. Brewster ME, Loftsson T. *Adv Drug Deliv Rev* 59: 645-666 (2007)

87. Del Valle EMM. *Process Biochem* 39: 1033-1046 (2004)

88. Fenyvesi É. Cyclodextrin news. (2013) URL https://cyclolab.hu (accessed 11.18.19).

89. Loftsson T. Jarho P, Másson M, Järvinen T. *Expert Opin Drug Deliv* 2: 335-351 (2005)

90. Topuz F, Uyar T. *Pharmaceutics* 11: 6 (2019)

91. Zupancic S, Skrlec K, Kocbek P, Kristl J, Berlec A. *Pharmaceutics* 11: 183 (2019)

92. Persano L, Camposeo A, Tekmen C, Pisignano D. *Macromol Mater Eng* 298: 504-520 (2013)

93. Hirsch E, Vass P, Démuth B, Pethő Z, Bitay E, Andersen SK, Vigh T, Verreck G, Molnár K, Nagy ZK, Marosi G. *Express Polym Lett* 13: 590-603 (2019)

94. **Kiss K, Vass P, Farkas A, Hirsch E, Szabó E, Mező G, Nagy ZK, Marosi G.** *Int J Pharm* **586: 119539 (2020)**

95. Tomeh MA, Hadianamrei R, Zhao X. *Int J Mol Sci* 20: 103 (2019)

96. **Kiss K, Hegedüs K, Vass P, Vári-Mező D, Farkas A, Nagy ZK, Molnár L, Tóvári J, Mező G, Marosi G.** *Int J Pharm* **611: 121327 (2022)**

97. **Pethő L, Kasza G, Lajkó E, Láng O, Kőhidai L, Iván B, Mező G.** *Soft Matter* **16: 5759-5769 (2020)**

98. Kasza G, Kali G, Domján A, Pethő L, Szarka G, Iván B. *Macromolecules* 50: 3078 (2017)

99. Li Z, Zhao R, Wu X, Sun Y, Yao M, Li J, Xu Y, Gu J. *FASEB J* 19: 1978 (2005)

100. Song S, Liu D, Peng J, Deng H, Guo Y, Xu LX, Miller AD, Xu Y. *FASEB J* 23: 1396 (2009)

101. **Mező G, Hegedüs K, Kiss K, Szakács G, Füredi A, Varga Z, Tóth S, Barta G, Nagyné Nalzályi L. EP4056169A1 (EU Patent) (2022)**